A lipid droplet-peroxisome network drives longevity by monounsaturated fatty acids via modulating ether lipid synthesis and ferroptosis

Anne Brunet (anne.brunet@stanford.edu)
Stanford University https://orcid.org/0000-0002-4608-6845
Katharina Papsdorf
Stanford University
Amir Hosseini
Stanford University
Jason Miklas
Stanford University https://orcid.org/0000-0002-9002-0667
Matias Cabruja
Stanford University
Yong Yu
Xiamen University
Luke Meraz Murphy
Stanford University
Carlos Silva-Garcia
Harvard T. H. Chan School of Public Health
Pallas Yao
Harvard University
Elisa de Launoit
Stanford University
William Mair
Harvard University https://orcid.org/0000-0002-0661-1342
Meng Wang
Baylor College of Medicine/Howard Hughes Medical Institute https://orcid.org/0000-0002-5898-6007
Michael Snyder
Stanford University https://orcid.org/0000-0003-0784-7987

Biological Sciences - Article

Keywords: mono-unsaturated fatty acids, organelle hub, lipid droplet

Posted Date: August 13th, 2021

DOI: https://doi.org/10.21203/rs.3.rs-740521/v1

A lipid droplet-peroxisome network drives longevity by monounsaturated fatty acids via modulating ether lipid synthesis and ferroptosis

Katharina Papsdorf[1], Amir Hosseini[1], Jason W. Miklas[1], Matias Cabruja[1], Yong Yu[2,3], Luke Meraz Murphy[1], Carlos Silva Garcia[4], Pallas Yao[4], Elisa de Launoit[1], William B. Mair[4], Meng C. Wang[2,5], Michael P. Snyder[1], Anne Brunet[1,6,#]

[1]Department of Genetics, Stanford University, Stanford, CA94305, USA
[2]Department of Molecular and Human Genetics, Huffington Center on Aging, Baylor College of Medicine, Houston, TX77030, USA
[3]Present address: School of Life Sciences, Xiamen University, China
[4]Department of Molecular Metabolism, Harvard, Boston, MA02115, USA
[5]Howard Hughes Medical Institute, Baylor College of Medicine, Houston, TX77030, USA
[6]Glenn Laboratories for the Biology of Aging, Stanford University, Stanford, CA94305, USA
[#]Correspondence: Anne Brunet, anne.brunet@stanford.edu

Abstract

Dietary mono-unsaturated fatty acids (MUFAs) are linked to human longevity and extend lifespan in several species[1-12]. But the mechanisms by which MUFAs promote longevity remain unclear. Here we show that an organelle hub involving lipid droplets and peroxisomes is critical for lifespan extension by MUFAs in *C. elegans*. MUFA accumulation increases lipid droplet number in fat storage tissues, and lipid droplet synthesis is necessary for MUFA-mediated longevity. Interestingly, the number of lipid droplets in young individuals can predict their remaining lifespan. MUFA accumulation also increases the number of peroxisomes, and peroxisome activity is required for MUFA-mediated longevity. By performing a targeted screen, we uncover a functional network between lipid droplets and peroxisomes in longevity. Interestingly, our screen also identifies ether lipids as critical components of the lipid droplet-peroxisome network. Using lipidomics, we find that the ratio of MUFAs to polyunsaturated fatty acids (PUFAs) in ether lipids is increased by MUFA accumulation. Ether lipids are involved in ferroptosis, a non-apoptotic form of cell death[13-17], and MUFAs promote longevity in part via suppression of ferroptosis. Our results identify a mechanism of action for MUFAs to extend lifespan and uncover an organelle network involved in the homeostasis of MUFA-rich ether lipids. Our work also opens new avenues for lipid-based interventions to delay aging.

Main

Lifespan is strongly influenced by diet. High fat diets are mostly detrimental for lifespan, but specific lipids can be beneficial for health and longevity[18-21]. Diets that are rich in monounsaturated fatty acids (MUFAs), such as olive oil in the Mediterranean diet, are correlated with longevity in humans[1,2]. Specific MUFAs (e.g. oleic acid and palmitoleic acid) causally extend lifespan in species ranging from *C. elegans* to mammals[3,4,6-11]. Yet the mechanism by which some lipids promote longevity, while others are detrimental for health, remain unknown.

Attractive candidates for the mechanism of MUFA action are conserved organelles involved in fat storage and metabolism, such as lipid droplets[22-24]. While the role of lipid droplets has started to be evaluated during aging, age-related diseases, and the response to stressors in different species[25-34], it is still unclear whether these organelles are positive or negative regulators of health. However, the importance of lipid droplets in MUFA-mediated longevity, and their mechanism of action for lifespan extension, is unknown.

We asked whether MUFAs influence lipid droplets in *C. elegans*, and whether this is critical for lifespan extension. To precisely assess lipid droplet number, we used Stimulated Raman Scattering (SRS) – a spectroscopy method that enables label-free imaging of lipids by visualizing carbo-hydrogen bonds[35-39]. MUFA accumulation was induced by upregulating SCD1/FAT-7, the enzyme that produces MUFAs (via knock-down of the chromatin regulator *ash-2* [ref[6]]), or by downregulating FAT-2, the enzyme that catabolizes MUFAs[6,10] (Fig. 1a). These manipulations indeed led to lifespan extension and MUFA accumulation (Extended Data Fig.1a, b, c)[5,6,10]. Interestingly, MUFA accumulation by *ash-2* or *fat-2* knock-down resulted in increased number of lipid droplets in intestinal cells, the main fat storage cells in *C. elegans* (Fig. 1b, c). These lipid droplets were not only more numerous, but they also had higher SRS intensity (Extended Data Fig. 1d), indicating they were more packed with lipids. We independently confirmed that MUFA enrichment led to increased lipid droplet number using a transgenic strain that expresses the lipid droplet membrane protein DHS-3 fused to GFP[40-42] (Fig. 1d, e). Males also showed increased lipid droplet number in the intestine upon MUFA accumulation (Fig. 1f, Extended Data Fig. 1e), indicating the effect of MUFAs on lipid droplets generalizes across sexes. MUFA accumulation led to lipid droplet accumulation in intestine cells, but not in other cells (e.g. hypodermis or eggs) (Fig. 1g, h, Extended Data Fig. 1f, g), and it did not impact lipid droplet *size* in a uniform manner (Extended Data Fig. 1h, i). Thus, MUFA accumulation results in increased lipid droplet number in lipid storage tissues.

Importantly, dietary supplementation with oleic acid, a cis MUFA present in olive oil and nuts, increased intestinal lipid droplet number and extended lifespan (Fig. 1i, j, k, l). In contrast, dietary supplementation with elaidic acid, a trans MUFA present in margarine and dairy and known to have detrimental effects on human health[43], did not increase lipid droplet number and did not extend lifespan (Fig. 1j, k, l). Hence, cis MUFA (but not trans MUFA) supplementation triggers an increase lipid droplet number, which correlates with lifespan extension.

To test if increased lipid droplet number is necessary for MUFAs to extend lifespan, we inhibited lipid droplet synthesis by targeting genes involved in this process (Fig. 1m). Knock-down of *LIPIN1/lpin-1*, which is important for the synthesis of lipid droplets[44-50] (Fig. 1n), resulted in fewer lipid droplets in both basal and MUFA-enriched conditions (Fig. 1n, o, Extended Fig. 1j, l). Interestingly, *lpin-1* deficiency blunted longevity by MUFA accumulation due to *ash-2* depletion (Fig. 1p) or oleic acid supplementation (Fig. 1q). Consistently, deficiency in *SEIPIN/seip-1*, which is implicated in the early steps of lipid droplet biogenesis[51-55] (Fig. 1m), also abolished lipid droplet increase in response to MUFA accumulation by *ash-2* RNAi (Extended Fig. 1m, n), and *seip-1* mutants no longer exhibit lifespan extension in response to MUFA accumulation by *ash-2* or *fat-2* RNAi (Fig. 1r, s). Collectively, our data indicate that an increase in lipid droplet number is necessary for MUFAs to extend lifespan.

Is the increase in lipid droplet number sufficient for longevity and could it predict remaining lifespan in a population of individuals? Depletion of *HSL1/hosl-1* or *ATGL/atgl-1*, which are involved in lipid droplet hydrolysis (see Fig. 1m)[24,56-58], led to an increase in lipid droplet number and a slight but significant lifespan extension (Fig. 2a, b, Extended Data Fig. 2a, b). These data suggest that increased lipid droplet number is sufficient to extend lifespan, even in the absence of MUFAs.

To determine if a high lipid droplet number can predict a long lifespan, we assessed the lifespan of genetically identical individuals with varying amounts of lipid droplets in a population of *C. elegans* individuals. We used the large particle BioSorter[59,60] to sort two subpopulations of young adult worms expressing high or low fluorescent levels of the lipid droplet marker fused to GFP (Fig. 2c, Extended Data Fig. 2c). Higher fluorescence worms indeed had more lipid droplets compared to lower fluorescence ones (Fig. 2d, e). Interestingly, individuals with more lipid droplets lived significantly longer than individuals with less lipid droplets (Fig. 2f). The predictive power of lipid droplet number for longevity was even more evident when the worms were sorted at middle age (Fig. 2g, h, Extended Data Fig. 2d). Thus, increased lipid droplet number is sufficient to extend lifespan and can predict remaining lifespan, consistent with a beneficial role for lipid droplets in longevity.

We next probed the mechanism by which lipid droplets extend lifespan in response to MUFAs. Lipid droplets interact with other organelles, such as mitochondria and peroxisomes, to regulate lipid metabolism[23,61-65] (Fig. 3a). Re-analysis of transcriptomic datasets of *C. elegans* with or without MUFA accumulation[5,6] showed peroxisome-related GO terms in conditions of MUFA accumulation (Fig. 3b). Peroxisomes have been shown to regulate longevity in *C. elegans* and *Drosophila* in some contexts[66,67], but their role in longevity by dietary fatty acids and their relationship with lipid droplets for lifespan extension is unknown. Using transgenic reporter strain that carries GFP fused to a peroxisome import signal[66,68], we found that MUFA accumulation due to *ash-2 and fat-2* depletion led to increased number and intensity of peroxisomes (Fig. 3c, d, Extended Data Fig. 3a, b, c, d). Depletion of the peroxisomal protein importer *prx-5* or the peroxisome membrane protein importer *prx-19* blunted peroxisome increase in response to MUFAs (Extended Data Fig. 3e), and this deficiency in peroxisome activity abolished longevity due to *ash-2* knock-down or dietary oleic acid supplementation (Fig. 3e, Extended Data Fig. 3f, g). Hence, peroxisome activity is required for longevity in response to MUFA accumulation.

We next examined the relationship between lipid droplets and peroxisomes in response to MUFA accumulation. Lipid droplet number correlated with peroxisome number in individual worms (Extended Data Fig. 3h). Furthermore, both organelles exhibited similar dynamics with age and in response to MUFA accumulation (Fig. 3f), with an increase in young adults followed by a decrease at middle age (Extended Data Fig. 3i, j).

Lipid droplets and peroxisomes can form physical contacts[65,69], but how they influence each other functionally – especially in the context of longevity – remains unknown. To understand the functional connection between lipid droplets and peroxisomes, we performed a targeted screen to identify genes that impact lipid droplet and peroxisome number. We tested 50 genes known to be involved in metabolism, or present in lipid droplets or peroxisomes[40,41,47,55,65,68,70-82] (Fig. 3g). There was a striking correlation between peroxisome and lipid droplet numbers upon perturbation of proteins involved in metabolism, lipid droplet, and peroxisome function (Fig. 3h), consistent with a joint regulation of these organelles. Perturbations that led to more lipid droplets and peroxisomes were often those that resulted in lifespan extension (Fig. 3h). Interestingly, our screen also uncovered the genes *ads-1* and *fard-1* as hits that, when knocked-down, reduce both lipid droplet and peroxisome numbers (Fig.3i-l). ADS-1 and FARD-1 are involved in the synthesis of a specific form of lipids, called ether lipids, which have an ether bond instead of the more traditional ester bond (see Fig. 4d)[79]. These data reveal a functional hub between lipid droplets and peroxisomes in longevity and identify ether lipid synthesis as an important regulator of this network.

Is ether lipid synthesis important for longevity by MUFAs? Deficiency in the ether lipid synthesis gene *ads-1* and *fard-1* blunted the lifespan extension due to MUFA accumulation upon *ash-2* and *fat-2* depletion (Fig. 3m, Extended Data Fig. 3k, l). Ether lipid synthesis also abolished the ability of lipid droplet increase due to *hosl-1* depletion or sorting to extend lifespan (Fig. 3n, Extended Data Fig. 3m). While the decrease in lipid droplet and peroxisome number by *ads-1* and *fard-1* knock-down could lead to this reduction in longevity, these data also raise the possibility that ether lipid synthesis plays a role in longevity by MUFA accumulation. In contrast, depletion of enzymes related to peroxisomal beta oxidation (*daf-22*)[68,72,83-85] or hydrogen peroxide degradation (*ctl-3*)[86] were not required for lifespan extension by MUFA accumulation (Extended Data Fig. 3n, o). Collectively, these data reveal a connection between lipid droplets and peroxisomes for longevity and highlight ether lipids as being important for lifespan.

Ether lipids are present in several lipid classes, including triglycerides and phospholipids, and they can modulate ferroptosis[13-16], a form of cell death due to iron accumulation, in both *C. elegans* and mammalian cells[87,88] (see Fig. 4g). We first asked how ether lipids (and other lipids) change in response to MUFA accumulation. To this end, we performed lipidomics on worms treated with *ash-2* RNAi to induce MUFA accumulation, in the presence or absence of peroxisome deficiency (*prx-5* RNAi) (Fig 4a). As expected, *ash-2* RNAi led to a global increase in MUFAs and triglycerides (Fig. 4b, Extended Data Fig 4a), and this was abolished when peroxisome function was inhibited (Fig. 4b, Extended Data Fig 4a). Principal component analysis (PCA) on all lipid species easily separated samples with MUFA enrichment (*ash-2* RNAi) and with peroxisome deficiency (*prx-5* RNAi) (Fig. 4c). Many lipids were remodeled in response to MUFA accumulation by *ash-2* knock-down with or without peroxisome function (see Extended Data Table 6 and Methods), providing a great resource for lipid composition changes under these conditions. Importantly, ether lipids were one of the major lipids driving the separation between MUFA-enriched samples with and without peroxisome function (Fig. 4c, PC1).

MUFAs and PUFAs can be incorporated into ether lipids (Fig. 4d), and PUFA-containing ether lipids are known to be detrimental[13,14]. While MUFA accumulation led to a decrease in total ether lipid levels (Extended Data Fig 4b), it actually increased the MUFA to PUFA ratio among ether lipids (Fig. 4e, f, Extended Data Fig 4c). The class of lipids that contains most ether bonds were the membrane lipids phosphatidylethanolamine (PE) (Extended Data Fig 4d), and MUFA accumulation also led to a significant increase in the MUFA to PUFA ratio among ether lipids in PEs (Fig. 4f, Extended Data Fig 4e). Thus, MUFA accumulation may be beneficial by increasing the ratio of MUFAs to PUFAs among ether lipids, thereby off-setting the negative impact of PUFA-containing ether lipids.

Ether lipids are involved in ferroptosis, an iron-dependent form of cell death characterized by accumulation of lipid peroxides[13-15,89,90] (Fig. 4g). We asked whether modulating ferroptosis could impact MUFA-mediated longevity. To induce ferroptosis, we depleted the glutathione peroxidase *GPX4/gpx-1*, which normally protects from lipid peroxidation and ferroptosis[91] (Fig. 4g). Interestingly, *gpx-1* knock-down blocked longevity due to *ash-2* knock-down (Fig. 4h), suggesting that protection from ferroptosis is required for MUFA-mediated longevity. To block ferroptosis, we used the iron-chelating drug Salinazid[88]. We found that Salinazid extended *C. elegans* lifespan, as previously shown[88], but could not further extend the long lifespan of *ash-2* or *fat-2* deficient worms (Fig 4i, Extended Data Fig. 4f). These results are consistent with the possibility that MUFAs extend lifespan by inhibiting ferroptosis. Finally, deficiency in lipid droplets (*lpin-1* RNAi) or ether lipid synthesis (*ads-1* RNAi) abolished Salinazid-mediated longevity (Fig. 4 j, k). These results suggest that the beneficial effect of blocking ferroptosis on lifespan also requires intact lipid metabolism, perhaps because an appropriate ratio of MUFAs vs. PUFAs among ether lipids is critical. Together, our results suggest that MUFAs extend lifespan by increasing the number of lipid droplets and peroxisomes, which could impact the ratio of MUFAs vs. PUFAs among ether lipids and result in the inhibition of ferroptotic death.

Our study identifies a mechanism of action by which dietary fatty acids extend lifespan and uncovers the importance of a lipid droplet-peroxisome organelle hub in longevity. We find that high lipid droplet and peroxisome number is beneficial for longevity by monounsaturated fatty acids such as oleic acid (present in olive oil) and a high lipid droplet number in young individuals can even predict remaining longevity. The role of lipid droplets in longevity was not clear, with studies indicating beneficial effects but others showing detrimental effects. For example, in *Drosophila*, expression of a protein that tethers lipid droplets is beneficial for short-term survival in response to starvation and is associated with high median lifespan[30], and lipid droplet composition can protect stem cell niches from damaging lipid peroxidation[29]. Moreover, lipid droplets can release MUFAs, which in turn activate beneficial metabolic enzymes and transcriptional regulators[34]. Lipid droplets have also been found to act as innate immune hubs that can kill pathogens[92]. In contrast, lipid droplets also accumulate during old age and disease[93] and are detrimental in many contexts[25-27,31,33,94-96]. Furthermore, conditions that lead to fat storage but also lipolysis have been associated with longevity[42,97-114]. Our results may point to conditions (i.e. intact peroxisome function) that are needed for a high lipid droplet number to be beneficial for health.

We find that lipid droplet numbers at two different adult ages are predictive of remaining lifespan. Increased levels of reactive oxygen species during early development are also predictive of remaining lifespan, in part by reducing chromatin marks (e.g. those deposited by ASH-2)[59]. Early life events may also act determine lifespan trajectories by modulating MUFAs and rely on an intact lipid droplet-peroxisome network. This result is also intriguing in light of the observation that among dietary restricted individuals (in mice or humans)[115,116], the fattest ones are the longest lived.

Our data reveal a functional connection between lipid droplets and peroxisomes in longevity. While physical interactions have been identified between lipid droplets and peroxisomes[65,69], a functional connection – especially in the context of aging – was not known. This hub between lipid droplets and peroxisomes appears to involve specific lipid – ether lipids – and it may be critical not only in aging, but also in other biological processes or diseases.

Finally, we also show for the first time that ether lipids regulate longevity, in part by modulating ferroptosis – a conserved form of cell death[16,89,90]. MUFAs have been found to protect from ferroptosis by displacing PUFAs from membrane lipids in mammalian cells[117]. It is possible that a high MUFA diet changes the balance among ether lipids in cells and prevent non-apoptotic forms of cell death in the organism. Given the conservation of lipid metabolism and organelles in all species, our findings open new avenues – based on lipid metabolism and composition – for promoting longevity and health.

Methods

C. elegans and bacteria strains

All *C. elegans* strains (N2 wild-type and mutants) used in this study are listed in Extended Data Table 4. Worms from mutant deletion strains were genotyped by PCR, and PCR amplicon sizes were used to check for deletions. *C. elegans* were grown and maintained at 20°C on standard Nematode Growth Media (NGM) plates seeded with a lawn of OP50-1 (gift from Dr. M.-W. Tan). For all experiments, worms were grown at 20°C on RNAi plates seeded with the RNAi strains HT115 (DE3) or the RNAi-sensitized iOP50 (gift from Dr. M. Wang) for ferroptosis induction by *gpx-1* deletion. Some strains were provided by the CGC, which is funded by NIH Office of Research Infrastructure Programs (P40 OD010440) and the Mitani Laboratory at the Tokyo Women's Medical University School of Medicine.

The WBM1177 strain, which expresses a peroxisome localization sequence (SKL) fused to GFP driven by the *eft-3* promoter, was generated by microinjection using CRISPR into WBM1140 (wbmIs65 [eft-3p::3XFLAG::dpy-10 crRNA::unc-54 3'UTR]) using the SKI LODGE system[118]. This system allows for knock-in of a single-copy of the construct downstream of the *eft-3* promoter, which drives gene expression in all somatic cells and allows for ubiquitous expression of peroxisome-targeted GFP.

RNA interference

For knockdown by RNA interference (RNAi), worms were fed HT115 (DE3) (and in a few cases iOP50 bacteria) transformed with vectors expressing double-stranded RNA against the gene of interest. The bacteria HT115 strains expressing RNAi against the gene of interest were obtained from the Ahringer library (gift from Dr. A. Fire). RNAi clones were confirmed by sequencing. Experiments were performed on HT115 unless noted otherwise.

To generate RNAi-expressing bacteria, a single bacterial colony was used to inoculate LB containing 100 µg/ml ampicillin (Sigma Aldrich). The bacterial culture was grown overnight at 37°C to stationary phase and the expression of the double stranded RNAi was induced with 0.4 mM IPTG (Thermo Fisher) for 4h at 37°C. The cultures were centrifuged, and concentrated 30x by resuspending the bacterial pellet in $LB_{Amp/IPTG}$ (LB with 100 µg/ml ampicillin, 0.4 mM IPTG) at 1:30 of the initial volume. This bacterial resuspension was stored at 4°C for no longer than two weeks. Concentrated bacteria were added to 6-cm or 10-cm agar plates/KPO_4 containing 100 µg/ml ampicillin and 0.4 mM IPTG (RNAi plates). For knockdown experiments, worms were kept on 6-cm plates seeded with RNAi-expressing bacteria. Unless indicated otherwise, worms were fed the RNAi from egg lay on. For *lpin-1* and *fat-2*, the RNAi was initiated at adult day one (young adult) to minimize effects of these gene knockdowns on development. For a negative control, worms were fed the empty-vector (L4440) bacteria strain. When 2 genes were knocked down simultaneously, the OD_{600} of the bacteria was adjusted to the same value ($OD_{600} = 50$, stationary phase) and the RNAi expressing bacteria were mixed in a 1:1 ratio. To assess the gene knockdown efficiency in the context of single versus double RNAi, we performed real time quantitative PCR (RT-qPCR) with primers to each gene of interest (Extended Data Figure 1k), as indicated below in the "Real time quantitative PCR" section.

Real time quantitative PCR

To test the efficiency of gene knockdown in the context of single versus double RNAi, quantitative RT-PCR was performed as described[6]. Briefly, 300 worms were subjected to RNAi-expressing bacteria (or control bacteria) on 6-cm RNAi plates. For experiments with *lpin-1* RNAi, knockdown for all conditions was initiated at young adult age and worms were harvested at adult day 2. Worms were washed 3 times with M9 buffer (22 mM KH_2PO_4, 34 mM K_2HPO_4, 86 mM NaCl, 1mM $MgSO_4$) to remove residual bacteria in the worm pellet. To isolate total RNA, worm pellets were resuspended in 500 µl Trizol Reagent (Invitrogen) and subjected to six freeze-thaw cycles in a dry ice-ethanol bath. RNA was extracted according to the standard Trizol procedure, resuspended in 30 µl of RNase- and DNase- free water, and quantified using the Nanodrop (Thermo Fisher). RNA was treated with DNAse (Thermo Fisher, Cat#:18068015), followed by reverse-transcription using Oligo $(dT)_{20}$ primers (Invitrogen, 18418020) and SuperScript IV Reverse Transcriptase (Invitrogen,18090010). iTaq^{TM} Universal SYBR Green super mix (Bio-Rad,1725124) was used in a 20 µl reaction volume for the real time quantitative PCR reaction. Primers were designed to span exon-exon junctions and used at a final concentration of 250 nM. All primers are listed in Extended Data Table 5. Real time quantitative PCR was performed using the C1000 thermal cycler (Bio-Rad). Melt curves were examined to ensure specificity of qPCR primers. Results were analyzed using the ΔΔ-CT method. For each biological replicate, the median Ct value of 3 technical replicates was analyzed and *act-1* served as the internal reference gene. Bar plots were plotted using Prism 8. Experiment was performed twice independently, with 3 replicates each. Statistical significance was tested using the unpaired, non-parametric Mann-Whitney test.

Scattered Raman Spectroscopy for lipid droplet quantification

To visualize all lipids in a label-free way, we used Stimulated Raman Scattering (SRS) microscopy[35]. Individual worms (treated with control or RNAi-expressing HT115 bacteria) were imaged post reproduction at adult day 6 (middle-age). Worms were mounted on a 2% agar pad, anesthetized with 50 mM sodium azide and covered with a glass cover slide for imaging. Worms were imaged directly after mounting to avoid confounds from starvation on the microscope slide using an SRS setup as described previously[119]. The experimental set-up was built on an inverted microscope (IX81, Olympus, Shinjuku, Japan). For SRS microscopy, spatially and temporally overlapped pulsed Pump (tunable from 720 to 990 nm, 7 ps, 80 MHz repetition rate) and Stokes (1064 nm, 5 ~ 6 ps, 80 MHz repetition rate, modulated at 8 MHz) beams provided by picoEMERALD (Applied Physics & Electronics, Berlin, Germany) were coupled into an inverted laser-scanning microscope (FV1000 MPE; Olympus) optimized for near-IR throughput. A 20× air objective (UPlanSAPO; 0.75N.A.; Olymp) and a 60x water objective (UPlanAPO/IR; 1.2N.A.; Olympus) were used for imaging. After passing through the sample, the forward going Pump and Stokes beams were collected in transmission by an air condenser (0.9 N.A., Olympus) for the 20x magnification and an oil condenser (1.4 N.A., Olympus) for the 60x magnification. A high OD bandpass filter (890/220, Chroma, Bellows Falls, VT) was used to block the Stokes beam completely and to transmit only the Pump beam onto a large area Si photodiode (FDS1010, Thorlabs) to for the detection of the stimulated Raman loss signal. The output current from the photodiode was terminated, filtered, and demodulated by a lock-in amplifier (HF2LI; Zurich

Instruments, Zurich, Switzerland) at 8 MHz to ensure shot noise-limited detection sensitivity. The laser power of IR and OPO were set at 600 mW. For lipid imaging, CH_2 signals from lipid droplets were imaged at 2845 cm^{-1} in SRS channel. These settings are used to visualize all lipids, as they are rich in these type of bonds. For lipid droplet imaging, one experiment was recorded at 60x and the duplicate was recorded using a 20x objective. Within one replicate, the same threshold was applied to all images and lipid droplets were quantified in a 26 x 26 μm^2 area using the analyze particle function in Fiji version 2.0.0 (Ref [120]). Experiments were not performed in a blinded manner. For each experiment, n>18 hermaphrodites were imaged per conditions, and the experiment was carried out in 2 independent experiments. Lipid droplet numbers and intensities were plotted using dot plots in Prism 8 and statistically significant differences between samples were assessed using the unpaired, non-parametric Mann-Whitney test.

Confocal microscopy for lipid droplet quantification

To visualize lipid droplets by confocal microscopy, we used a reporter strain expressing the lipid droplet protein DHS-3 fused to green fluorescent protein (GFP), which has been previously characterized as a lipid droplet marker[40,41]. Transgenic LIU1 (*dhs-3p::DHS-3::GFP*) worms were imaged post reproduction at adult day 6, unless noted otherwise. For each experiment, ~20 worms were imaged per condition. Worms were mounted on a 2% agar pad, anesthetized with 50 mM sodium azide and covered with a glass cover slide for imaging. Worms were imaged with the Nikon Eclipse Ti confocal microscope with a Zyla sCMOS camera (Andor) and NIS-Elements software (AR 4.30.062, 64 bit) using the 100x oil objective (Nikon, Plan Apo, 100x) or a Zeiss confocal microscope (LSM900, Axio Observer) using the 63x oil objective (Plan-Apochromat) and Zen software (3.0, blue). The mid-intestinal region was imaged in 0.2 µm slices and all images were taken using the same exposure time. Lipid droplet numbers were analyzed in Fiji version 2.0.0 (Ref [120]) by generating z-stack projections of 5 slices, applying the same threshold to all images and manually counting the lipid droplets in a 26 x 26 μm^2 area. Lipid droplet diameters were analyzed in Fiji version 2.0.0 (Ref [120]) by generating z-stack projections of 5 slices, applying the same threshold to all images and manually measuring the diameter of all lipid droplets in focus.

To measure lipid droplets in males, transgenic LIU1 (*dhs-3p::DHS-3::GFP*) males were generated by a brief 1h heat shock of L4 hermaphrodites at 36°C. The male progeny were picked and maintained by crossing them with hermaphrodites. For all other steps, male worms were processed similarly as described above.

To measure hypodermal lipid droplets, transgenic LIU2 (*plin-1p::PLIN-1::mCherry*) worms were imaged post reproduction at adult day 6. This reporter strain has been used to visualize hypodermal and intestinal lipid droplets[40]. For each experiment, ~20 worms were imaged per condition. Worms were processed similarly as described above with the following differences. To analyze hypodermal lipid droplets, the head hypodermis was imaged to avoid accidently imaging intestinal lipid droplets. As the width of the worms is smaller in the head region, a smaller area 15 x 15 area μm^2 was selected to count the number of lipid droplets.

To visualize lipid droplets in eggs, nile red staining was performed as described before[41]. Briefly, adult day 1 hermaphrodites were fixed in 40% isopropanol for 3 minutes and stained with 8 µM nile red (MP biomedicals # 0215174450) for 2 hours in the dark. Worms were mounted and imaged similarly as described before. One to two fertilized eggs per worm were imaged *in utero* in 0.2 µm slices. For each experiment, ~20 worms were imaged per condition. The number of lipid droplets was counted in a 16 x 16 μm^2 area using the Squassh plugin[121]. The following plugin settings were used and kept consistent across experiments. The background was subtracted with a rolling ball radius of 10 pixels, the segmentation parameters were set at 0.005 with a minimum object intensity of 0.15.

All experiments and lipid droplet analysis were performed in a blinded manner. Each experiment was at least carried out twice independently. Lipid droplet numbers and intensities were plotted using dot plots in Prism 8 and statistically significant differences between samples were assessed using the unpaired, non-parametric Mann-Whitney test.

Monounsaturated fatty acid supplementation

To increase the level of specific fatty acids in *C. elegans*, we performed dietary supplementation as described before[6]. In short, fatty acid sodium derivatives (Nu-check prep) of oleic acid (C18:1n9 cis) and elaidic acid (C18:1n9 trans) were dissolved in water at 100 mM. To dissolve elaidic acid, the solution was heated in a water bath to 50°C for no more than 10 minutes. The detergent Tergitol (NP-40, Sigma Aldrich) was added at a concentration of 0.001% to RNAi agar plates prior to autoclaving. After autoclaving, the agar media plates were cooled down to approximately 60°C and the fatty acids solutions were added to a final concentration of 0.8 mM. The agar media was stirred for 2 minutes after addition of the fatty acids to ensure even distribution. The plates were dried overnight in a dark ventilates space, stored at 4°C and used within a month. Bacteria were seeded on oleic acid or elaidic acid plates 24 hours before worms were transferred to the plates. For supplementation experiments, worms were kept on oleic acid or elaidic acid plates from egg lay on. For experiments including *lpin-1* knock-down, RNAi and fatty acid supplementation were both started simultaneously at adult day 1 because of the negative effect of *lpin-1* knock-down on development.

Lifespan assays

All *C. elegans* lifespan assays were performed at 20°C on RNAi plates. Hermaphrodites were age-synchronized with a short 4 hour egg lay using synchronized young (adult day 1) parents. Hermaphrodites were transferred to new plates and scored at least every other day to avoid the presence of confounding progeny. Each lifespan assay was performed with 3 plates of ~30 worms per 6-cm RNAi plates (~90 worms total). Worms were scored as censored if they crawled off the media or if they died upon vulval rupture/internal hatching. Worms were scored as dead when they failed to move upon gentle prodding with a platinum wire pick (90% Pt, 10% Ir). For lifespan curves, censored worms were included until the day of censorship. All lifespan experiments were performed in a blinded and randomized manner. Each experiment was carried out at least twice independently. Kaplan-Meier survival curves were plotted in Prism 8. For pairwise comparison, the log-rank (Mantel-Cox) statistical test in Prism was used. To test if two interventions significantly interact with each other, the Cox proportional hazard test was applied using R (Version 3.6.3). For all lifespan statistics, see Extended Data Table 1.

Gas chromatography/mass spectrometry analysis of fatty acid profiles

To ensure that fatty acid profiles change upon *ash-2* RNAi, targeted gas chromatography/mass spectrometry (GC/MS) was performed as described before[6]. Briefly, for each condition, approximately 500 age-synchronized adult day 1 animals were collected in M9 buffer and washed 3 times to remove residual bacteria in the worm pellets. Worm pellets were lyzed by sonication and protein concentration of the lysate was determined using the Pierce BCA Protein Assay Kit (Thermo- Scientific). The fatty acid C13:0 (NuChek Prep, dissolved in methanol), was added to each sample to serve as the internal reference control for variations introduced during derivatization and extraction steps. Fatty acids were derivatized into their respective fatty acid methyl ester (FAME) by incubation in 2% H_2SO_4 (Sigma Aldrich) in methanol (Fisher) at 55°C overnight. The reaction was stopped by the addition of 1.5 ml water (Fisher, MS grade). FAMEs were extracted in a 300 µl hexane (Sigma Aldrich) by vigorous vortexing and centrifuging at 1000 rpm for 1 minute. The hexane layer, containing the FAMEs, was transferred into an amber GC vial (Agilent). FAME analysis was performed using an Agilent 7890A gas chromatograph equipped with an HP-5MS column. Each FAME peak was identified based on its retention time and unique fragmentation ions and quantified using a serial dilution standard curve.

FAME abundance measured by GC-MS was normalized to the internal C13:0 reference control of each sample. For each sample FAMEs concentration (µg/ml) was normalized to protein concentration (mg/ml) as microgram of fatty acid detected per milligram of protein (µg/mg). The fatty acid concentration (µg/mg) for *ash-2* RNAi was normalized to the fatty acid concentration (µg/mg) of the empty vector control. The final ratio is expressed as relative fatty acid levels in the graph. Each experiment was at least carried out twice independently. Relative fatty acid abundances were plotted Prism 8 and statistically significant differences between samples were assessed using the unpaired, non-parametric Mann Whitney test with Benjamini and Hochberg test for multiple hypothesis correction.

Separating fluorescent worms using the BioSorter

To sort worms according to their lipid droplet number at young age (adult day 1), we used the large particle BioSorter (Union Biometrica). To retrieve a large number of age-synchronized worms for the sorting procedure, approximately 5,000 eggs were laid by age-synchronized adult day 1 parent worms expressing DHS-3 fused to GFP (*dhs-3p*::DHS-3::GFP, LIU1). After approximately 72 hours at 20°C, the laid eggs developed into adult worms that were collected in M9 buffer (22 mM KH_2PO_4, 34 mM K_2HPO_4, 86 mM NaCl, 1mM $MgSO_4$) and sorted on the large particle flow cytometer BioSorter (Union Biometrica) with a 6.5 psi sample cup pressure, 2.00 psi diverter pressure, 50% sheath flow rate, rotary valve, 8.0 ms drop width and 10.0 ms sort delay using the FlowPilot III software. Using a dissecting microscope, we visually confirmed these settings enabled us to sort the accurate number of worms. The highest and lowest 10% fluorescent worms of the population were sorted using the 488 nm laser (Extended Data Fig. 2c). Worms were directly sorted onto 6-cm RNAi plates containing a bacterial lawn

(HT115, empty vector). We confirmed that the sorting reflects the lipid droplet number by fluorescence confocal microscopy (Fig. 2d, e). For this, worms were mounted on a 2% agar pad, anesthetized with 50 mM sodium azide and covered with a glass cover slide for imaging. Worms were imaged with the Nikon Eclipse Ti confocal microscope with a Zyla sCMOS camera (Andor) and NIS-Elements software (AR 4.30.062, 64 bit) using the 100x oil objective (Nikon, Plan Apo, 100x) or a Zeiss confocal microscope (LSM900, Axio Observer) using the 63x oil objective (Plan-Apochromat) and Zen software (3.0, blue). Lipid droplet quantification was performed blinded and as described above. Each experiment was performed at least twice independently. BioSorter graphs were plotted using the FlowPilot III software, and confocal microscopy quantifications were plotted in Prism 8. Statistically significant differences between samples were assessed using the unpaired, non-parametric Mann-Whitney test.

Separating fluorescent worms using manual sorting

To sort worms according to their fluorescence at middle age, we manually separated high and low fluorescent worms on a fluorescent dissecting microscope. To retrieve a large number of age-synchronized worms for the sorting procedure, approximately 5,000 eggs were laid by age-synchronized adult day 1 parent worms (*dhs-3p*::DHS-3::GFP, LIU1). After approximately 72 hours at 20°C, the eggs developed into adult worms. The adult worms were washed each day during their reproductive period to separate the adult worms from larvae/eggs. For this, worms were collected in M9 buffer (22 mM KH_2PO_4, 34 mM K_2HPO_4, 86 mM NaCl, 1mM $MgSO_4$) in a 15 ml tube and allowed to settle to the bottom of the tube. The supernatant was removed and worms were resuspended in 15 ml of fresh M9. This washing procedure was repeated 5 times and the adult worms were transferred to fresh 10 cm RNAi plates seeded with 1 ml empty vector HT115 bacteria. Post-reproductive middle-aged worms (adult day 6, no noticeable egg production) were sorted under a fluorescent dissecting microscope (Leica M165 FC) equipped with a Sola light engine (Leica) on 6-cm RNAi plates containing a bacterial lawn (HT115, empty vector). We confirmed that the sorting reflects the lipid droplet number by fluorescence confocal microscopy (Fig. 2g). Worms were mounted on a 2% agar pad, anesthetized with 50 mM sodium azide and covered with a glass cover slide for imaging. Worms were imaged with the Nikon Eclipse Ti confocal microscope with a Zyla sCMOS camera (Andor) and NIS-Elements software (AR 4.30.062, 64 bit) using the 100x oil objective (Nikon, Plan Apo, 100x) or a Zeiss confocal microscope (LSM900, Axio Observer) using the 63x oil objective (Plan-Apochromat) and Zen software (3.0, blue). Lipid droplet quantification was performed blinded and as described above. Each experiment was performed at least twice independently. Graphs were plotted using dot plots in Prism 8. Statistically significant differences between samples were assessed using the unpaired, non-parametric Mann-Whitney test.

Re-analysis of gene expression datasets

We re-analyzed two independent gene expression datasets that were generated previously in the lab, and we tested GO term enrichment in conditions that lead to MUFA accumulation. First, we analyzed a RNA-seq dataset from the intestine of adult day 1 worms treated with *ash-2* RNAi[6]. We selected the genes that had a log2 fold-enrichment larger than 1 (42 genes/adjusted *P*-value<0.05) and analyzed enrichment for GO terms using WormEnrichR[122,123]. All categories of GO terms were included in subsequent analysis. Second, we analyzed a microarray dataset from the entire body of post-reproductive worms treated with *ash-2* RNAi[5]. We selected the genes that were had a log2 fold-enrichment larger than 1 (304 genes/adjusted p-value<0.05) and analyzed enrichment for GO terms using WormEnrichR for GO terms. All categories of GO terms were included in subsequent analysis. Significantly enriched GO terms (combined score >5)[122-124] that were shared between the two datasets were plotted using R (Version 3.6.3). Duplicated GO terms were deleted based on the higher combined score in the RNAseq dataset. The combined score was calculated by multiplying the *P*-value retrieved from the Fisher's Exact test with the z-score. For detailed list of all GO terms, see Extended Data Table 2.

Confocal microscopy for peroxisome quantification

Peroxisomes were visualized by confocal microscopy using worm strains that express a fluorophore fused to a peroxisome localization sequence (SKL). The fluorophore was either GFP for *ges-1p::GFP-SKL*(VS15) and *eft-3p::GFP-SKL* (WBM1177) or mRFP for *vha-6p::mRFP-SKL; dsh-3p::DHS-3::GFP* (ABR161). Transgenic worms were imaged post-reproduction at adult day 6, unless noted otherwise. The last intestinal cell was imaged in a similar way as described before[66]. We used these cells for quantification because they retain homogenous fluorophore expression with age. Worms were mounted on a 2% agar pad, anesthetized with 50 mM sodium azide and covered with a glass cover slide for imaging. Worms were imaged with the Nikon Eclipse Ti confocal microscope with a Zyla sCMOS camera (Andor) and NIS-Elements software (AR 4.30.062, 64 bit) using the 100x objective or a Zeiss confocal microscope (LSM900, Axio Observer) using the 63x oil objective (Plan-Apochromat) and Zen software (3.0, blue). The last intestinal cell was imaged in 0.2 µm slices and all images were taken using the same exposure time. Images were analyzed in Fiji version 2.0.0 (Ref [120]) by generating z-stack projections of 5 slices, applying the same threshold to all images and automatically counting the lipid droplets in a 26 x 26 μm^2 area using the Squassh plugin[121]. This plugin was used to count the numbers of particles and analyze their fluorescence intensity. The following settings were used and kept consistent across experiments. The background was subtracted with a rolling ball radius of 10, the segmentation parameters were set at 0.005 with a minimum object intensity of 0.15. Peroxisomes usually appeared as fluorescent puncta. Rarely, when the fluorophore was only cytosolic and failed to localize to peroxisomes, the plugin did not perform correctly, and these quantifications were excluded from further analysis. All experiments and analysis were performed in a blinded manner unless noted otherwise in the Source Data Tables. For each experiment, ~20 worms were imaged per condition. Each experiment was performed at least twice independently. Peroxisome numbers were plotted using dot plots in Prism 8 and statistically significant differences between samples were tested using the unpaired, non-parametric Mann-Whitney test.

Lipid droplet and peroxisome number as a function of age

To visualize lipid droplet and peroxisome dynamics as a function of age, we imaged worms during their adult life. Lipid droplets and peroxisomes were visualized by confocal microscopy at different ages and quantified as described above. Peroxisomes were visualized by mRFP and lipid droplets by GFP in the *vha-6p::mRFP-SKL; dsh-3p::DHS-3::GFP* (ABR161) double marker strain as described above. The last intestinal cells were imaged as described above. Lipid droplet and peroxisome numbers were quantified using the same region of interest per worm. All experiments and analysis were performed in a blinded manner. For each experiment, ~24 worms were imaged per condition. Experiments carried out twice independently. Mean organelle numbers and regression lines were plotted using Prism 8.

Targeted lipid droplet and peroxisome screen

To analyze how lipid droplet genes influence peroxisome numbers and vice versa, we performed a targeted RNAi screen. We selected genes to target for the screen based on proteins identified by mass spectrometry at the surface of lipid droplets[40,41] and based on annotated protein function in lipid metabolism, lipid droplet biology, and peroxisome biology. As a positive control, we used *ash-2* RNAi and *prx-5* RNAi. We assessed the effect of RNAi knock-down of these genes on lipid droplet and peroxisome numbers at day 6 of life in approximately 30 animals per condition. Lipid droplets and peroxisomes were visualized by confocal microscopy and quantified as described above. The screen was performed in six groups. Each group contained the empty vector control, *ash-2* and *prx-5* RNAi. Peroxisomes were visualized by mRFP (except for the first group) and lipid droplets by GFP in the *vha-6p::mRFP-SKL; dsh-3p::DHS-3::GFP* (ABR161) double-marker strain. For the first group, peroxisomes were measured in another set of worms, using the single marker strain *ges-1p::GFP-SKL (VS15)* and the corresponding lipid droplet numbers were from an independent experiment. For all other groups, lipid droplet and peroxisome numbers were quantified using the same 26x26 μm^2 area region of interest per worm in the last intestinal cell. Organelle numbers were normalized to the control empty vector RNAi within the corresponding group. Lipid droplet numbers were quantified manually and peroxisome numbers were quantified using the Squassh plugin[121] as described above. Peroxisomes usually appear as puncta. Rarely, when the fluorophore was only cytosolic and failed to localize to peroxisomes, the plugin did not perform correctly, and these quantifications were excluded from further analysis. All experiments and analysis were performed in a blinded manner. To assess correlation of organelle numbers, the mean organelle number normalized to the control condition (empty vector RNAi) was plotted using Prism and statistically significant correlation was tested using the Pearson's r test. Manhattan graphs were plotted using Prism8 and statistical significance was tested using a two-tailed Mann-Whitney test and Benjamini-Hochberg correction was used for multiple hypothesis correction.

Sample preparation for lipidomics

To analyze lipid composition using mass spectrometry, hermaphrodites were treated with control (empty vector) RNAi, *prx-5* RNAi, *ash-2* RNAi, and *prx-5/ash-2* double RNAi until middle-age (adult day 6). Each condition consists of six biological replicates. To retrieve a large number of age-synchronized worms for the procedure, approximately 500 eggs were laid by age-synchronized adult day 1 wildtype parents per replicate plate. After 2 hours of egg laying, the parents were removed and the plates were checked that no parents remained. Once the worms reached the young adult stage, they were washed each day to separate the adult worms from larvae/eggs. For this, worms were collected in M9 buffer (22 mM KH_2PO_4, 34 mM K_2HPO_4, 86 mM NaCl, 1mM $MgSO_4$) and allowed to settle to the bottom of the tube. The supernatant was removed and fresh M9 was added. This washing procedure was repeated 6 times and the adult worms were transferred to fresh 6-cm RNAi plates seeded with 500 µl RNAi-expressing HT115 bacteria. At middle-age (adult day 6), worms were transferred to empty RNAi plates without any bacteria for 15 minutes, to clear residual bacteria in the gut. Worms were then collected in 200 µl M9 in protein-low bind Eppendorf tubes (cat # 13-698-794). Worms were lyzed using a pre-chilled stainless-steel homogenizer (Wheaton, cat # 357572) and were homogenized with 10 plunger strokes. The lysate (from approximately 500 worms) was frozen on dry ice and stored at -80°C.

Lipid isolation for mass spectrometry

Lipids from the whole worm lysates were extracted using a biphasic separation with methyl tert-butyl ether (MTBE), methanol and water[125]. All reagents used are for lipidomics are LC/MS grade. Briefly, 298 µl of ice-cold methanol and 2 µl of internal standard (equiSPLASH, Avanti Polar Lipids, cat# 330731) were added to 50 µl of worm lysate. The mixture was vortexed for 20 seconds and 1000 µl of ice-cold MTBE was added. The mixture was incubated under agitation for 30 minutes at 4°C. After addition of 250 µl of water, the samples were vortexed for 1 minute and centrifuged at 14,000 g for 10 minutes at room temperature. The upper phase containing the lipids was collected and dried down under nitrogen. The dry extracts were reconstituted with 300 µl of 9:1 methanol:toluene (Fisher Scientific) with 10 mM of ammonium acetate (Sigma Aldrich) and centrifuged at 14,000 g for 5 minutes before analysis. Water extracted using the same protocol was used as a blank control. Samples were randomized in all cases during lipid extraction.

Liquid chromatography mass spectrometry

To identify complex lipids, isolated lipids were analyzed with untargeted lipidomics using liquid chromatography coupled to a Q Exactive mass spectrometer (Thermo Fisher Scientific) (LC/MS). Lipids were separated using an Accucore C30 column 2.1 x 150 mm, 2.6 µm (Thermo Scientific, cat# 27826-152130) and mobile phase solvents consisted in 1 mM ammonium formate and 0.1% formic acid in 60/40 acetonitrile/water (A) and 1 mM ammonium formate and 0.1% formic acid in 90/10 isopropanol/acetonitrile (B). The gradient profile used was 30% B for 3 minutes, 30–43% B over 5 minutes, 43–50% B over 1 minute, 55–90% B over 9 minutes, 90-

99% B over 9 minutes and 99% B for 5 minutes. Lipids were eluted from the column at 0.2 ml/min, the oven temperature was set at 30°C, and the injection volume was 15 μl. Autosampler temperature was set at 15°C to prevent lipid aggregation. The Q Exactive plus was equipped with a HESI-II probe and operated in full MS scan mode for all the samples. MS/MS spectra were acquired in data-dependent acquisition mode on pooled samples. The source conditions were as follows: Spray Voltage = 3.5 kV (ESI positive mode), Vaporizer = 200°C, Capillary Temperature = 375°C, S-Lens = 55.0%, SheathGas = 40, Auxiliary gas = 8, SweepGas = 0. The acquisition settings were as follows: AGC (MS) = 3e6, AGC (MS^2) = 1e5, Maximum Injection Time (MS) = 200 ms, Maximum Injection Time (MS^2) = 50 ms, Mass Range = 260–1,900 Da, Resolution MS = 70,000 (FWHM at m/z 200), Resolution MS^2 = 35,000 (FWHM at m/z 200), MS^2 spectra was acquired in top-10 ions in each cycle, Isolation Window = 1.0 m/z, Dynamic Exclusion = 12 s, Normalized Collision Energy (NCE) = 25–30. External calibration was performed using an infusion of Pierce LTQ Velos ESI Positive Ion Calibration Solution.

Analysis of mass spectrometry results

Lipid species were identified by matching the precursor ion mass to a database and the experimental MS/MS spectra to a spectral library containing theoretical fragmentation spectra using LipidSearch software version 4.1 (Thermo Scientific)[126]. Further data processing was done using an in-house analysis pipeline written in R (Version 3.6.3, available in Github at https://github.com/brunetlab).

Briefly, processing for samples and spike-in standards were done in the same way. All ions for one lipid were aggregated and lipids with a signal >0 discarded from further analysis. Lipid species were quantified using the corresponding internal standard (equiSPLASH, Avanti Polar Lipids, cat# 330731) for each lipid class. Lipids with signals lower than 3x blank signal were discarded. Lipids with more than 50% of missing values were discarded and for the remaining missing values, imputation was performed. For this, a value was randomly assigned based on the bottom 5% for the corresponding lipid. Lipids were filtered for a coefficient of variance <0.5. Each sample was divided by its corresponding protein concentration to correct for sample input variations. To calculate normalized abundance, each lipid within a sample was divided by the sample median followed by multiplication with the global median. This resulted in a total of 500 filtered and normalized lipids belonging to 16 lipid classes. For a complete list of all lipidomic data, see Extended Data Table 6. Changes in the most abundant lipid classes – diacyglycerol

(DG), phosphatidylethanolamine (PE), phosphatidylcholine (PC) and phosphatidylinositol (PI) – as well as differences in abundance of fatty acids grouped by length are listed in Source Data Extended Data Fig 4 and Extended Data Table 7. Together, these data indicate that peroxisome deficiency widely remodels the lipidome, with accumulation of long-chain fatty acids, in agreement with a previously published study[127]. We also observed an increase in saturated fatty acids upon peroxisome deficiency (Fig. 4b), consistent with previous studies that detected an increase in saturated long-chain fatty acids upon peroxisome deficiency[128,129]. Box plots were plotted using R (Version 3.6.3). Statistical significance was tested using a two-tailed Mann-Whitney test and Benjamini-Hochberg correction was used for multiple hypothesis correction. To test if two interventions significantly interact with each other, a two-way ANOVA was applied using Prism8.

Role of ferroptosis in longevity by MUFAs and lipid droplets

To test the effect of ferroptosis – a non-apoptic form of cell death involving oxidized lipids – on lifespan, we modulated the ferroptosis process in *C. elegans*. To induce ferroptosis, we performed RNAi knock-down of the *gpx-1* gene, which encodes a glutathione peroxidase. As ferroptosis induction was shown to be enhanced on an OP50 diet (compared to an HT115 diet)[15,130], we fed *gpx-1(tm2100)* mutants with iOP50 bacteria[131] expressing *ash-2* and control empty vector (L4440) RNAi. To inhibit ferroptosis, we exposed worms to Salinazid (LGC Standards/Dr. Ehrenstorfer cat # DRE-C16904350), a lipophilic compound that scavenges intracellular iron, thereby inhibiting iron-triggered lipid peroxidation that induce ferroptosis[88,132]. Salinazid was dissolved in DMSO and added to autoclaved RNAi media before solidification to a final concentration of 250 μM. Plates were dried overnight in a dark ventilated space, stored at 4°C, and used within a month. Worms were transferred to Salinazid and control (DMSO) plates, at adult day 1. Lifespan was measured as described above.

Statistics

No statistical method was used to predetermine sample size. Parameters such as the minimum n value, mean ± standard deviation and significant *P-values* are reported in the figures, the figure legends or the corresponding source files. Significance was defined by a *P-value* < 0.05. All *P-values* can be found in the source data tables. Pairwise comparisons were made using the Mann Whitney test (also called Wilcoxon rank sum test) in Prism8. When over five comparisons were made, the Benjamini-Hochberg correction was used for multiple hypothesis correction. When testing for correlation, the Pearson correlation test was used and normality distribution was confirmed using the Kolmogorov-Smirnov test using Prism8. To test if two interventions interact with each other, a two-way ANOVA was applied using Prism8.

For pairwise comparison of lifespan data, the log-rank (Mantel-Cox) statistical test in Prism8 was used. To test if two lifespan interventions significantly interact with each other, the Cox proportional hazard test was applied using R (Version 3.6.3) which was reported in the figure legends. All lifespan statistics are reported in Extended Data Table S1. Statistical analyses were performed using Prism8 or R (Version 3.6.3).

Acknowledgements

We thank the Stanford Mass Spectrometry facility (Vincent Coates Foundation Mass Spectrometry Laboratory) and Dr. Allis Chien for GC/MS use and support. We thank the Stanford High Throughput BioCenter and Dr. David E. Solow-Cordero for BioSorter use and support *(*supported by NIH SIG S10OD025004). We thank the Brunet Lab, and in particular Drs. Lauren N. Booth, Paloma Navarro and Xiaoai Zhao for their feedback and reading of the manuscript. We thank Drs. Andrew S. McKay and Xiaoai Zhao for independently checking scripts used in this study. We thank Drs. Jonathan Long and Scott Dixon for insightful discussion and for critical reading of the manuscript. This work was supported by R01AG054201 (A.B., W.B.M.), a DFG German Research Foundation postdoctoral fellowship (K.P.), and a Hillblom Foundation postdoctoral fellowship (J.W.M.).

Authors contributions

K.P. and A.B. planned the study. K.P. performed and analyzed all experiments, except for those indicated below. A.H. performed and analyzed the peroxisome quantification, targeted screen, independent repeats of lifespan experiments, and Salinazid experiments. J.W.M. performed the peroxisome sorting experiment and participated in the planning of the study. M.C. ran and analyzed the lipidomics samples supervised by M.P.S. L.M.M. and E.D.L. helped K.P. with data collection on lipid droplet and peroxisome number, respectively. Y.Y. performed and analyzed the SRS experiments supervised by M.C.W. C.G.G. generated several *C. elegans* lines and P.Y. generated the WBM1177 line supervised by W.B.M., and C.G.G. and W.B.M. also had intellectual input in the study. K.P. and A.B. wrote the manuscript, and all authors provided comments.

Competing Interests

The authors declare no competing interests.

Data availability

All data generated or analyzed during this study are included in this published article (and its supplementary information files). All lipidomic files are available in the Github repository for this paper (https://github.com/brunetlab/Papsdorf_etal_2021).

Code availability

The code used to analyze lipidomic data in the current study are available in the Github repository for this paper (https://github.com/brunetlab/Papsdorf_etal_2021).

References

1 Tosti, V., Bertozzi, B. & Fontana, L. Health Benefits of the Mediterranean Diet: Metabolic and Molecular Mechanisms. *J Gerontol A Biol Sci Med Sci* **73**, 318-326, doi:10.1093/gerona/glx227 (2018).

2 Mendez, M. A. & Newman, A. B. Can a Mediterranean Diet Pattern Slow Aging? *J Gerontol A Biol Sci Med Sci* **73**, 315-317, doi:10.1093/gerona/gly003 (2018).

3 Hansen, M., Flatt, T. & Aguilaniu, H. Reproduction, fat metabolism, and life span: what is the connection? *Cell Metab* **17**, 10-19, doi:10.1016/j.cmet.2012.12.003 (2013).

4 Broughton, S. J. *et al.* Longer lifespan, altered metabolism, and stress resistance in Drosophila from ablation of cells making insulin-like ligands. *Proc Natl Acad Sci U S A* **102**, 3105-3110, doi:10.1073/pnas.0405775102 (2005).

5 Greer, E. L. *et al.* Members of the H3K4 trimethylation complex regulate lifespan in a germline-dependent manner in C. elegans. *Nature* **466**, 383-387, doi:10.1038/nature09195 (2010).

6 Han, S. *et al.* Mono-unsaturated fatty acids link H3K4me3 modifiers to C. elegans lifespan. *Nature* **544**, 185-190, doi:10.1038/nature21686 (2017).

7 Folick, A. *et al.* Aging. Lysosomal signaling molecules regulate longevity in Caenorhabditis elegans. *Science* **347**, 83-86, doi:10.1126/science.1258857 (2015).

8 O'Rourke, E. J., Kuballa, P., Xavier, R. & Ruvkun, G. omega-6 Polyunsaturated fatty acids extend life span through the activation of autophagy. *Genes Dev* **27**, 429-440, doi:10.1101/gad.205294.112 (2013).

9 Qi, W. *et al.* The omega-3 fatty acid alpha-linolenic acid extends Caenorhabditis elegans lifespan via NHR-49/PPARalpha and oxidation to oxylipins. *Aging Cell* **16**, 1125-1135, doi:10.1111/acel.12651 (2017).

10 Yuan, Y. *et al.* Enhanced energy metabolism contributes to the extended life span of calorie-restricted Caenorhabditis elegans. *J Biol Chem* **287**, 31414-31426, doi:10.1074/jbc.M112.377275 (2012).

11 Goudeau, J. *et al.* Fatty acid desaturation links germ cell loss to longevity through NHR-80/HNF4 in C. elegans. *PLoS Biol* **9**, e1000599, doi:10.1371/journal.pbio.1000599 (2011).

12 Choi, L. S., Shi, C., Ashraf, J., Sohrabi, S. & Murphy, C. T. Oleic Acid Protects Caenorhabditis Mothers From Mating-Induced Death and the Cost of Reproduction. *Front Cell Dev Biol* **9**, 690373, doi:10.3389/fcell.2021.690373 (2021).

13 Cui, W., Liu, D., Gu, W. & Chu, B. Peroxisome-driven ether-linked phospholipids biosynthesis is essential for ferroptosis. *Cell Death Differ*, doi:10.1038/s41418-021-00769-0 (2021).

14 Zou, Y. *et al.* Plasticity of ether lipids promotes ferroptosis susceptibility and evasion. *Nature* **585**, 603-608, doi:10.1038/s41586-020-2732-8 (2020).

15 Perez, M. A., Magtanong, L., Dixon, S. J. & Watts, J. L. Dietary Lipids Induce Ferroptosis in Caenorhabditiselegans and Human Cancer Cells. *Dev Cell* **54**, 447-454.e444, doi:10.1016/j.devcel.2020.06.019 (2020).

16 Cao, J. Y. & Dixon, S. J. Mechanisms of ferroptosis. *Cell Mol Life Sci* **73**, 2195-2209, doi:10.1007/s00018-016-2194-1 (2016).

17 Aldrovandi, M. & Conrad, M. Ferroptosis: the Good, the Bad and the Ugly. *Cell Res* **30**, 1061-1062, doi:10.1038/s41422-020-00434-0 (2020).

18 Mutlu, A. S., Duffy, J. & Wang, M. C. Lipid metabolism and lipid signals in aging and longevity. *Dev Cell* **56**, 1394-1407, doi:10.1016/j.devcel.2021.03.034 (2021).

19 Bustos, V. & Partridge, L. Good Ol' Fat: Links between Lipid Signaling and Longevity. *Trends Biochem Sci* **42**, 812-823, doi:10.1016/j.tibs.2017.07.001 (2017).

20 Schroeder, E. A. & Brunet, A. Lipid Profiles and Signals for Long Life. *Trends Endocrinol Metab* **26**, 589-592, doi:10.1016/j.tem.2015.08.007 (2015).

21 Puca, A. A., Chatgilialoglu, C. & Ferreri, C. Lipid metabolism and diet: possible mechanisms of slow aging. *Int J Biochem Cell Biol* **40**, 324-333, doi:10.1016/j.biocel.2007.04.003 (2008).

22 Gao, Q. & Goodman, J. M. The lipid droplet-a well-connected organelle. *Front Cell Dev Biol* **3**, 49, doi:10.3389/fcell.2015.00049 (2015).

23 Olzmann, J. A. & Carvalho, P. Dynamics and functions of lipid droplets. *Nat Rev Mol Cell Biol* **20**, 137-155, doi:10.1038/s41580-018-0085-z (2019).

24 Walther, T. C. & Farese, R. V., Jr. Lipid droplets and cellular lipid metabolism. *Annu Rev Biochem* **81**, 687-714, doi:10.1146/annurev-biochem-061009-102430 (2012).

25 Marschallinger, J. *et al.* Lipid-droplet-accumulating microglia represent a dysfunctional and proinflammatory state in the aging brain. *Nat Neurosci* **23**, 194-208, doi:10.1038/s41593-019-0566-1 (2020).

26 Gluchowski, N. L., Becuwe, M., Walther, T. C. & Farese, R. V., Jr. Lipid droplets and liver disease: from basic biology to clinical implications. *Nat Rev Gastroenterol Hepatol* **14**, 343-355, doi:10.1038/nrgastro.2017.32 (2017).

27 Liu, L. *et al.* Glial lipid droplets and ROS induced by mitochondrial defects promote neurodegeneration. *Cell* **160**, 177-190, doi:10.1016/j.cell.2014.12.019 (2015).

28 Geltinger, F. *et al.* The transfer of specific mitochondrial lipids and proteins to lipid droplets contributes to proteostasis upon stress and aging in the eukaryotic model system Saccharomyces cerevisiae. *Geroscience* **42**, 19-38, doi:10.1007/s11357-019-00103-0 (2020).

29 Bailey, A. P. *et al.* Antioxidant Role for Lipid Droplets in a Stem Cell Niche of Drosophila. *Cell* **163**, 340-353, doi:10.1016/j.cell.2015.09.020 (2015).

30 Ugrankar, R. *et al.* Drosophila Snazarus Regulates a Lipid Droplet Population at Plasma Membrane-Droplet Contacts in Adipocytes. *Dev Cell* **50**, 557-572.e555, doi:10.1016/j.devcel.2019.07.021 (2019).

31 Krahmer, N., Farese, R. V., Jr. & Walther, T. C. Balancing the fat: lipid droplets and human disease. *EMBO Mol Med* **5**, 973-983, doi:10.1002/emmm.201100671 (2013).

32 Mashek, D. G. Hepatic lipid droplets: A balancing act between energy storage and metabolic dysfunction in NAFLD. *Mol Metab*, 101115, doi:10.1016/j.molmet.2020.101115 (2020).

33 Ralhan, I., Chang, C. L., Lippincott-Schwartz, J. & Ioannou, M. S. Lipid droplets in the nervous system. *J Cell Biol* **220**, doi:10.1083/jcb.202102136 (2021).

34 Najt, C. P. *et al.* Lipid Droplet-Derived Monounsaturated Fatty Acids Traffic via PLIN5 to Allosterically Activate SIRT1. *Mol Cell* **77**, 810-824.e818, doi:10.1016/j.molcel.2019.12.003 (2020).

35 Ramachandran, P. V., Mutlu, A. S. & Wang, M. C. Label-free biomedical imaging of lipids by stimulated Raman scattering microscopy. *Curr Protoc Mol Biol* **109**, 30.33.31-30.33.17, doi:10.1002/0471142727.mb3003s109 (2015).

36 Chen, T., Yavuz, A. & Wang, M. C. Dissecting lipid droplet biology with coherent Raman scattering microscopy. *J Cell Sci* **135**, doi:10.1242/jcs.252353 (2022).

37 Mutlu, A. S., Chen, T., Deng, D. & Wang, M. C. Label-Free Imaging of Lipid Storage Dynamics in Caenorhabditis elegans using Stimulated Raman Scattering Microscopy. *J Vis Exp*, doi:10.3791/61870 (2021).

38 Chen, W. W. *et al.* Spectroscopic coherent Raman imaging of Caenorhabditis elegans reveals lipid particle diversity. *Nat Chem Biol* **16**, 1087-1095, doi:10.1038/s41589-020-0565-2 (2020).

39 Barros, A. G., Liu, J., Lemieux, G. A., Mullaney, B. C. & Ashrafi, K. Analyses of C. elegans fat metabolic pathways. *Methods Cell Biol* **107**, 383-407, doi:10.1016/b978-0-12-394620-1.00013-8 (2012).

40 Na, H. *et al.* Identification of lipid droplet structure-like/resident proteins in Caenorhabditis elegans. *Biochim Biophys Acta* **1853**, 2481-2491, doi:10.1016/j.bbamcr.2015.05.020 (2015).

41 Vrablik, T. L., Petyuk, V. A., Larson, E. M., Smith, R. D. & Watts, J. L. Lipidomic and proteomic analysis of Caenorhabditis elegans lipid droplets and identification of ACS-4 as a lipid droplet-associated protein. *Biochim Biophys Acta* **1851**, 1337-1345, doi:10.1016/j.bbalip.2015.06.004 (2015).

42 Daniele, J. R. *et al.* UPR(ER) promotes lipophagy independent of chaperones to extend life span. *Sci Adv* **6**, eaaz1441, doi:10.1126/sciadv.aaz1441 (2020).

43 Ganguly, R. & Pierce, G. N. Trans fat involvement in cardiovascular disease. *Mol Nutr Food Res* **56**, 1090-1096, doi:10.1002/mnfr.201100700 (2012).

44 Zhang, P. & Reue, K. Lipin proteins and glycerolipid metabolism: Roles at the ER membrane and beyond. *Biochim Biophys Acta Biomembr* **1859**, 1583-1595, doi:10.1016/j.bbamem.2017.04.007 (2017).

45 Donkor, J., Sariahmetoglu, M., Dewald, J., Brindley, D. N. & Reue, K. Three mammalian lipins act as phosphatidate phosphatases with distinct tissue expression patterns. *J Biol Chem* **282**, 3450-3457, doi:10.1074/jbc.M610745200 (2007).

46 Adeyo, O. *et al.* The yeast lipin orthologue Pah1p is important for biogenesis of lipid droplets. *J Cell Biol* **192**, 1043-1055, doi:10.1083/jcb.201010111 (2011).

47 Golden, A., Liu, J. & Cohen-Fix, O. Inactivation of the C. elegans lipin homolog leads to ER disorganization and to defects in the breakdown and reassembly of the nuclear envelope. *J Cell Sci* **122**, 1970-1978, doi:10.1242/jcs.044743 (2009).

48 Wang, H. *et al.* Lipin-1gamma isoform is a novel lipid droplet-associated protein highly expressed in the brain. *FEBS Lett* **585**, 1979-1984, doi:10.1016/j.febslet.2011.05.035 (2011).

49 Sellers, R. S., Mahmood, S. R., Perumal, G. S., Macaluso, F. P. & Kurland, I. J. Phenotypic Modulation of Skeletal Muscle Fibers in LPIN1-Deficient Lipodystrophic (fld) Mice. *Vet Pathol* **56**, 322-331, doi:10.1177/0300985818809126 (2019).

50 Jung, Y. *et al.* Caenorhabditis elegans Lipin 1 moderates the lifespan-shortening effects of dietary glucose by maintaining ω-6 polyunsaturated fatty acids. *Aging Cell* **19**, e13150, doi:10.1111/acel.13150 (2020).

51 Nettebrock, N. T. & Bohnert, M. Born this way - Biogenesis of lipid droplets from specialized ER subdomains. *Biochim Biophys Acta Mol Cell Biol Lipids* **1865**, doi:10.1016/j.bbalip.2019.04.008 (2020).

52 Szymanski, K. M. *et al.* The lipodystrophy protein seipin is found at endoplasmic reticulum lipid droplet junctions and is important for droplet morphology. *Proc Natl Acad Sci U S A* **104**, 20890-20895, doi:10.1073/pnas.0704154104 (2007).

53 Cartwright, B. R. *et al.* Seipin performs dissectible functions in promoting lipid droplet biogenesis and regulating droplet morphology. *Mol Biol Cell* **26**, 726-739, doi:10.1091/mbc.E14-08-1303 (2015).

54 Wang, H. *et al.* Seipin is required for converting nascent to mature lipid droplets. *Elife* **5**, doi:10.7554/eLife.16582 (2016).

55 Cao, Z. *et al.* Dietary fatty acids promote lipid droplet diversity through seipin enrichment in an ER subdomain. *Nat Commun* **10**, 2902, doi:10.1038/s41467-019-10835-4 (2019).

56 Zimmermann, R. *et al.* Fat mobilization in adipose tissue is promoted by adipose triglyceride lipase. *Science* **306**, 1383-1386, doi:10.1126/science.1100747 (2004).

57 Yang, L. *et al.* Neuronal lipolysis participates in PUFA-mediated neural function and neurodegeneration. *EMBO Rep* **21**, e50214, doi:10.15252/embr.202050214 (2020).

58 Sathyanarayan, A., Mashek, M. T. & Mashek, D. G. ATGL Promotes Autophagy/Lipophagy via SIRT1 to Control Hepatic Lipid Droplet Catabolism. *Cell Rep* **19**, 1-9, doi:10.1016/j.celrep.2017.03.026 (2017).

59 Bazopoulou, D. *et al.* Developmental ROS individualizes organismal stress resistance and lifespan. *Nature* **576**, 301-305, doi:10.1038/s41586-019-1814-y (2019).

60 Booth, L. N., Maures, T. J., Yeo, R. W., Tantilert, C. & Brunet, A. Self-sperm induce resistance to the detrimental effects of sexual encounters with males in hermaphroditic nematodes. *Elife* **8**, doi:10.7554/eLife.46418 (2019).

61 Rambold, A. S., Cohen, S. & Lippincott-Schwartz, J. Fatty acid trafficking in starved cells: regulation by lipid droplet lipolysis, autophagy, and mitochondrial fusion dynamics. *Dev Cell* **32**, 678-692, doi:10.1016/j.devcel.2015.01.029 (2015).

62 Nguyen, T. B. *et al.* DGAT1-Dependent Lipid Droplet Biogenesis Protects Mitochondrial Function during Starvation-Induced Autophagy. *Dev Cell* **42**, 9-21.e25, doi:10.1016/j.devcel.2017.06.003 (2017).

63 Valm, A. M. *et al.* Applying systems-level spectral imaging and analysis to reveal the organelle interactome. *Nature* **546**, 162-167, doi:10.1038/nature22369 (2017).

64 Cohen, S., Rambold, A. S. & Lippincott-Schwartz, J. Mitochondrial and Lipid Droplet Dynamics Regulate Intra- and Intercellular Fatty Acid Trafficking. *Mol Cell Oncol* **5**, e1043038, doi:10.1080/23723556.2015.1043038 (2018).

65 Chang, C. L. *et al.* Spastin tethers lipid droplets to peroxisomes and directs fatty acid trafficking through ESCRT-III. *J Cell Biol* **218**, 2583-2599, doi:10.1083/jcb.201902061 (2019).

66 Weir, H. J. *et al.* Dietary Restriction and AMPK Increase Lifespan via Mitochondrial Network and Peroxisome Remodeling. *Cell Metab* **26**, 884-896.e885, doi:10.1016/j.cmet.2017.09.024 (2017).

67 Huang, K. *et al.* Impaired peroxisomal import in Drosophila oenocytes causes cardiac dysfunction by inducing upd3 as a peroxikine. *Nat Commun* **11**, 2943, doi:10.1038/s41467-020-16781-w (2020).

68 Zhang, S. O. *et al.* Genetic and dietary regulation of lipid droplet expansion in Caenorhabditis elegans. *Proc Natl Acad Sci U S A* **107**, 4640-4645, doi:10.1073/pnas.0912308107 (2010).

69 Kong, J. *et al.* Spatiotemporal contact between peroxisomes and lipid droplets regulates fasting-induced lipolysis via PEX5. *Nat Commun* **11**, 578, doi:10.1038/s41467-019-14176-0 (2020).

70 Narayan, V. *et al.* Deep Proteome Analysis Identifies Age-Related Processes in C. elegans. *Cell Syst* **3**, 144-159, doi:10.1016/j.cels.2016.06.011 (2016).

71 Bersuker, K. *et al.* A Proximity Labeling Strategy Provides Insights into the Composition and Dynamics of Lipid Droplet Proteomes. *Dev Cell* **44**, 97-112.e117, doi:10.1016/j.devcel.2017.11.020 (2018).

72 Watts, J. L. & Ristow, M. Lipid and Carbohydrate Metabolism in Caenorhabditis elegans. *Genetics* **207**, 413-446, doi:10.1534/genetics.117.300106 (2017).

73 Boström, P. *et al.* SNARE proteins mediate fusion between cytosolic lipid droplets and are implicated in insulin sensitivity. *Nat Cell Biol* **9**, 1286-1293, doi:10.1038/ncb1648 (2007).

74 Chung, J. *et al.* LDAF1 and Seipin Form a Lipid Droplet Assembly Complex. *Dev Cell* **51**, 551-563.e557, doi:10.1016/j.devcel.2019.10.006 (2019).

75 Walther, T. C., Chung, J. & Farese, R. V., Jr. Lipid Droplet Biogenesis. *Annu Rev Cell Dev Biol* **33**, 491-510, doi:10.1146/annurev-cellbio-100616-060608 (2017).

76 Coppa, A. *et al.* The peroxisomal fatty acid transporter ABCD1/PMP-4 is required in the C. elegans hypodermis for axonal maintenance: A worm model for adrenoleukodystrophy. *Free Radic Biol Med* **152**, 797-809, doi:10.1016/j.freeradbiomed.2020.01.177 (2020).

77 Thieringer, H., Moellers, B., Dodt, G., Kunau, W. H. & Driscoll, M. Modeling human peroxisome biogenesis disorders in the nematode Caenorhabditis elegans. *J Cell Sci* **116**, 1797-1804, doi:10.1242/jcs.00380 (2003).

78 Choudhary, V., Ojha, N., Golden, A. & Prinz, W. A. A conserved family of proteins facilitates nascent lipid droplet budding from the ER. *J Cell Biol* **211**, 261-271, doi:10.1083/jcb.201505067 (2015).

79 Shi, X. *et al.* A Caenorhabditis elegans model for ether lipid biosynthesis and function. *J Lipid Res* **57**, 265-275, doi:10.1194/jlr.M064808 (2016).

80 Nguyen, T. B. & Olzmann, J. A. Getting a handle on lipid droplets: Insights into ER-lipid droplet tethering. *J Cell Biol* **218**, 1089-1091, doi:10.1083/jcb.201902160 (2019).

81 Joshi, A. S. & Cohen, S. Lipid Droplet and Peroxisome Biogenesis: Do They Go Hand-in-Hand? *Front Cell Dev Biol* **7**, 92, doi:10.3389/fcell.2019.00092 (2019).

82 Joshi, A. S. *et al.* Lipid droplet and peroxisome biogenesis occur at the same ER subdomains. *Nat Commun* **9**, 2940, doi:10.1038/s41467-018-05277-3 (2018).

83 Butcher, R. A. *et al.* Biosynthesis of the Caenorhabditis elegans dauer pheromone. *Proc Natl Acad Sci U S A* **106**, 1875-1879, doi:10.1073/pnas.0810338106 (2009).

84 Artyukhin, A. B. *et al.* Metabolomic "Dark Matter" Dependent on Peroxisomal β-Oxidation in Caenorhabditis elegans. *J Am Chem Soc* **140**, 2841-2852, doi:10.1021/jacs.7b11811 (2018).

85 Bouagnon, A. D. *et al.* Intestinal peroxisomal fatty acid β-oxidation regulates neural serotonin signaling through a feedback mechanism. *PLoS Biol* **17**, e3000242, doi:10.1371/journal.pbio.3000242 (2019).

86 Xie, M. & Roy, R. Increased levels of hydrogen peroxide induce a HIF-1-dependent modification of lipid metabolism in AMPK compromised C. elegans dauer larvae. *Cell Metab* **16**, 322-335, doi:10.1016/j.cmet.2012.07.016 (2012).

87 Lee, H. *et al.* Energy-stress-mediated AMPK activation inhibits ferroptosis. *Nat Cell Biol* **22**, 225-234, doi:10.1038/s41556-020-0461-8 (2020).

88 Jenkins, N. L. *et al.* Changes in ferrous iron and glutathione promote ferroptosis and frailty in aging Caenorhabditis elegans. *Elife* **9**, doi:10.7554/eLife.56580 (2020).

89 Jiang, X., Stockwell, B. R. & Conrad, M. Ferroptosis: mechanisms, biology and role in disease. *Nat Rev Mol Cell Biol* **22**, 266-282, doi:10.1038/s41580-020-00324-8 (2021).

90 Stockwell, B. R., Jiang, X. & Gu, W. Emerging Mechanisms and Disease Relevance of Ferroptosis. *Trends Cell Biol* **30**, 478-490, doi:10.1016/j.tcb.2020.02.009 (2020).

91 Forcina, G. C. & Dixon, S. J. GPX4 at the Crossroads of Lipid Homeostasis and Ferroptosis. *Proteomics* **19**, e1800311, doi:10.1002/pmic.201800311 (2019).

92 Bosch, M. *et al.* Mammalian lipid droplets are innate immune hubs integrating cell metabolism and host defense. *Science* **370**, doi:10.1126/science.aay8085 (2020).

93 Geltinger, F. *et al.* Friend or Foe: Lipid Droplets as Organelles for Protein and Lipid Storage in Cellular Stress Response, Aging and Disease. *Molecules* **25**, doi:10.3390/molecules25215053 (2020).

94 Ioannou, M. S. *et al.* Neuron-Astrocyte Metabolic Coupling Protects against Activity-Induced Fatty Acid Toxicity. *Cell* **177**, 1522-1535.e1514, doi:10.1016/j.cell.2019.04.001 (2019).

95 Shimabukuro, M. K. *et al.* Lipid-laden cells differentially distributed in the aging brain are functionally active and correspond to distinct phenotypes. *Sci Rep* **6**, 23795, doi:10.1038/srep23795 (2016).

96 Mosquera, J. V., Bacher, M. C. & Priess, J. R. Nuclear lipid droplets and nuclear damage in Caenorhabditis elegans. *PLoS Genet* **17**, e1009602, doi:10.1371/journal.pgen.1009602 (2021).

97 Lapierre, L. R., Gelino, S., Meléndez, A. & Hansen, M. Autophagy and lipid metabolism coordinately modulate life span in germline-less C. elegans. *Curr Biol* **21**, 1507-1514, doi:10.1016/j.cub.2011.07.042 (2011).

98 Seah, N. E. *et al.* Autophagy-mediated longevity is modulated by lipoprotein biogenesis. *Autophagy* **12**, 261-272, doi:10.1080/15548627.2015.1127464 (2016).

99 Lee, G. *et al.* Post-transcriptional Regulation of De Novo Lipogenesis by mTORC1-S6K1-SRPK2 Signaling. *Cell* **171**, 1545-1558.e1518, doi:10.1016/j.cell.2017.10.037 (2017).

100 Steinbaugh, M. J. *et al.* Lipid-mediated regulation of SKN-1/Nrf in response to germ cell absence. *Elife* **4**, doi:10.7554/eLife.07836 (2015).

101 Lynn, D. A. *et al.* Omega-3 and -6 fatty acids allocate somatic and germline lipids to ensure fitness during nutrient and oxidative stress in Caenorhabditis elegans. *Proc Natl Acad Sci U S A* **112**, 15378-15383, doi:10.1073/pnas.1514012112 (2015).

102 Lapierre, L. R., Meléndez, A. & Hansen, M. Autophagy links lipid metabolism to longevity in C. elegans. *Autophagy* **8**, 144-146, doi:10.4161/auto.8.1.18722 (2012).

103 Kim, H. E. *et al.* Lipid Biosynthesis Coordinates a Mitochondrial-to-Cytosolic Stress Response. *Cell* **166**, 1539-1552.e1516, doi:10.1016/j.cell.2016.08.027 (2016).

104 Higuchi-Sanabria, R. *et al.* Divergent Nodes of Non-autonomous UPR(ER) Signaling through Serotonergic and Dopaminergic Neurons. *Cell Rep* **33**, 108489, doi:10.1016/j.celrep.2020.108489 (2020).

105 Goh, G. Y. S. *et al.* NHR-49/HNF4 integrates regulation of fatty acid metabolism with a protective transcriptional response to oxidative stress and fasting. *Aging Cell* **17**, e12743, doi:10.1111/acel.12743 (2018).

106 Imanikia, S., Sheng, M., Castro, C., Griffin, J. L. & Taylor, R. C. XBP-1 Remodels Lipid Metabolism to Extend Longevity. *Cell Rep* **28**, 581-589.e584, doi:10.1016/j.celrep.2019.06.057 (2019).

107 Webster, C. M. *et al.* Genome-wide RNAi Screen for Fat Regulatory Genes in C. elegans Identifies a Proteostasis-AMPK Axis Critical for Starvation Survival. *Cell Rep* **20**, 627-640, doi:10.1016/j.celrep.2017.06.068 (2017).

108 Heimbucher, T., Hog, J., Gupta, P. & Murphy, C. T. PQM-1 controls hypoxic survival via regulation of lipid metabolism. *Nat Commun* **11**, 4627, doi:10.1038/s41467-020-18369-w (2020).

109 Zhang, P., Judy, M., Lee, S. J. & Kenyon, C. Direct and indirect gene regulation by a life-extending FOXO protein in C. elegans: roles for GATA factors and lipid gene regulators. *Cell Metab* **17**, 85-100, doi:10.1016/j.cmet.2012.12.013 (2013).

110 Littlejohn, N. K., Seban, N., Liu, C. C. & Srinivasan, S. A feedback loop governs the relationship between lipid metabolism and longevity. *Elife* **9**, doi:10.7554/eLife.58815 (2020).

111 Wang, M. C., O'Rourke, E. J. & Ruvkun, G. Fat metabolism links germline stem cells and longevity in C. elegans. *Science* **322**, 957-960, doi:10.1126/science.1162011 (2008).

112 Chen, A. L. *et al.* Pharmacological convergence reveals a lipid pathway that regulates C. elegans lifespan. *Nat Chem Biol* **15**, 453-462, doi:10.1038/s41589-019-0243-4 (2019).

113 Lee, D. *et al.* MDT-15/MED15 permits longevity at low temperature via enhancing lipidostasis and proteostasis. *PLoS Biol* **17**, e3000415, doi:10.1371/journal.pbio.3000415 (2019).

114 Soukas, A. A., Kane, E. A., Carr, C. E., Melo, J. A. & Ruvkun, G. Rictor/TORC2 regulates fat metabolism, feeding, growth, and life span in Caenorhabditis elegans. *Genes Dev* **23**, 496-511, doi:10.1101/gad.1775409 (2009).

115 Liao, C. Y. *et al.* Fat maintenance is a predictor of the murine lifespan response to dietary restriction. *Aging Cell* **10**, 629-639, doi:10.1111/j.1474-9726.2011.00702.x (2011).

116 Zheng, H., Echave, P., Mehta, N. & Myrskylä, M. Life-long body mass index trajectories and mortality in two generations. *Ann Epidemiol* **56**, 18-25, doi:10.1016/j.annepidem.2021.01.003 (2021).

117 Magtanong, L. *et al.* Exogenous Monounsaturated Fatty Acids Promote a Ferroptosis-Resistant Cell State. *Cell Chem Biol* **26**, 420-432.e429, doi:10.1016/j.chembiol.2018.11.016 (2019).

118 Silva-García, C. G. *et al.* Single-Copy Knock-In Loci for Defined Gene Expression in Caenorhabditis elegans. *G3 (Bethesda)* **9**, 2195-2198, doi:10.1534/g3.119.400314 (2019).

119 Yu, Y., Mutlu, A. S., Liu, H. & Wang, M. C. High-throughput screens using photo-highlighting discover BMP signaling in mitochondrial lipid oxidation. *Nat Commun* **8**, 865, doi:10.1038/s41467-017-00944-3 (2017).

120 Schindelin, J. *et al.* Fiji: an open-source platform for biological-image analysis. *Nat Methods* **9**, 676-682, doi:10.1038/nmeth.2019 (2012).

121 Rizk, A. *et al.* Segmentation and quantification of subcellular structures in fluorescence microscopy images using Squassh. *Nat Protoc* **9**, 586-596, doi:10.1038/nprot.2014.037 (2014).

122 Chen, E. Y. *et al.* Enrichr: interactive and collaborative HTML5 gene list enrichment analysis tool. *BMC Bioinformatics* **14**, 128, doi:10.1186/1471-2105-14-128 (2013).

123 Kuleshov, M. V. *et al.* Enrichr: a comprehensive gene set enrichment analysis web server 2016 update. *Nucleic Acids Res* **44**, W90-97, doi:10.1093/nar/gkw377 (2016).

124 Kuleshov, M. V. *et al.* modEnrichr: a suite of gene set enrichment analysis tools for model organisms. *Nucleic Acids Res* **47**, W183-w190, doi:10.1093/nar/gkz347 (2019).

125 Matyash, V., Liebisch, G., Kurzchalia, T. V., Shevchenko, A. & Schwudke, D. Lipid extraction by methyl-tert-butyl ether for high-throughput lipidomics. *J Lipid Res* **49**, 1137-1146, doi:10.1194/jlr.D700041-JLR200 (2008).

126 Taguchi, R. & Ishikawa, M. Precise and global identification of phospholipid molecular species by an Orbitrap mass spectrometer and automated search engine Lipid Search. *J Chromatogr A* **1217**, 4229-4239, doi:10.1016/j.chroma.2010.04.034 (2010).

127 Rackles, E. *et al.* Reduced peroxisomal import triggers peroxisomal retrograde signaling. *Cell Rep* **34**, 108653, doi:10.1016/j.celrep.2020.108653 (2021).

128 Chen, C. *et al.* Pex11a deficiency causes dyslipidaemia and obesity in mice. *J Cell Mol Med* **23**, 2020-2031, doi:10.1111/jcmm.14108 (2019).

129 Abe, Y., Honsho, M., Nakanishi, H., Taguchi, R. & Fujiki, Y. Very-long-chain polyunsaturated fatty acids accumulate in phosphatidylcholine of fibroblasts from patients with Zellweger syndrome and acyl-CoA oxidase1 deficiency. *Biochim Biophys Acta* **1841**, 610-619, doi:10.1016/j.bbalip.2014.01.001 (2014).

130 Perez, M. A., Magtanong, L., Dixon, S. J. & Watts, J. L. Dietary Induction and Modulation of Ferroptosis in Caenorhabditis elegans. *bioRxiv*, 772079, doi:10.1101/772079 (2019).

131 Neve, I. A. A. *et al.* Escherichia coli Metabolite Profiling Leads to the Development of an RNA Interference Strain for Caenorhabditis elegans. *G3 (Bethesda)* **10**, 189-198, doi:10.1534/g3.119.400741 (2020).

132 Kalinowski, D. S. & Richardson, D. R. The evolution of iron chelators for the treatment of iron overload disease and cancer. *Pharmacol Rev* **57**, 547-583, doi:10.1124/pr.57.4.2 (2005).

Figure 1

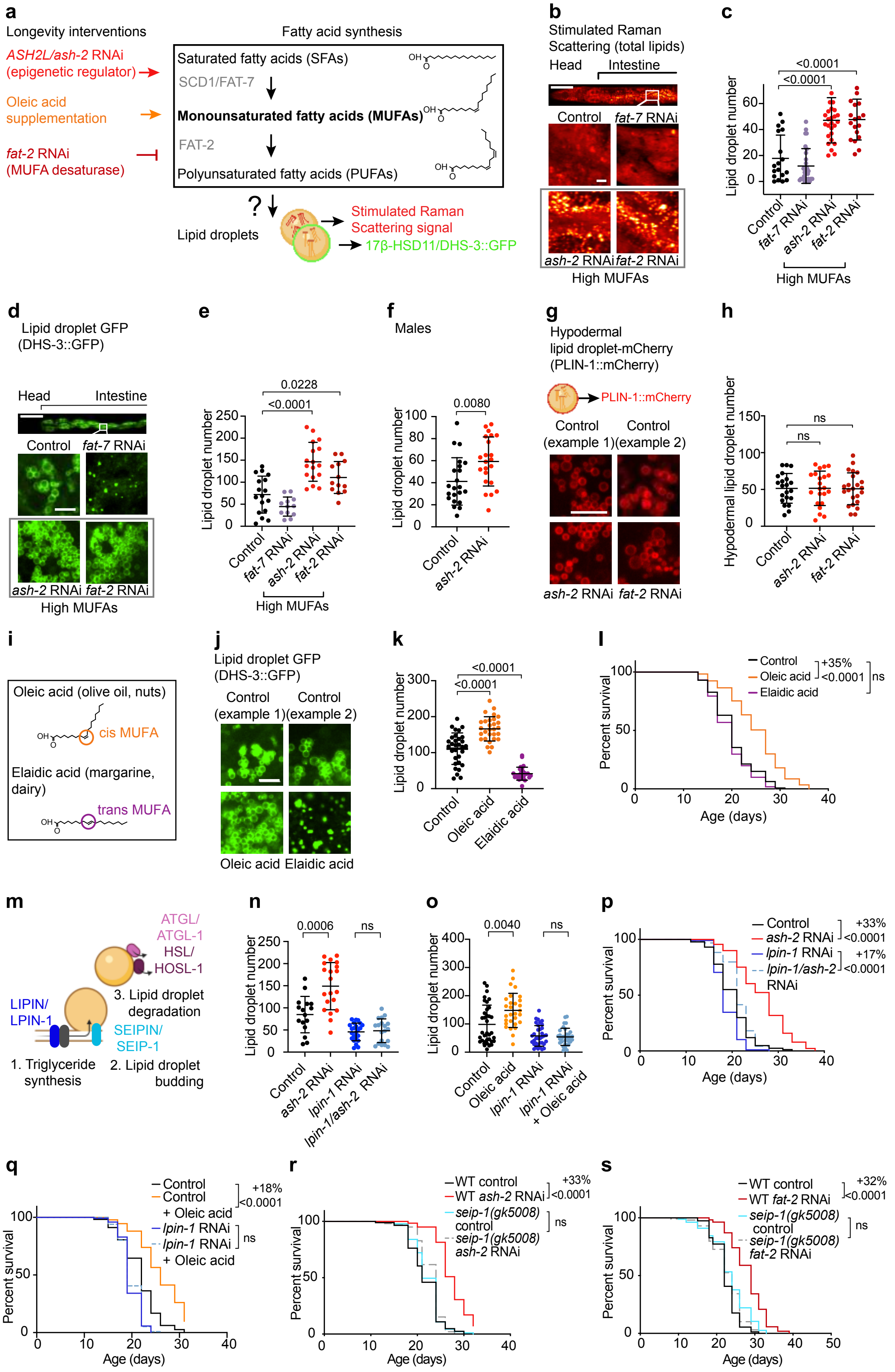
a
Longevity interventions
ASH2L/ash-2 RNAi
(epigenetic regulator)
Oleic acid
supplementation
fat-2 RNAi
(MUFA desaturase)
Fatty acid synthesis
Saturated fatty acids (SFAs)
SCD1/FAT-7
Monounsaturated fatty acids (MUFAs)
FAT-2
Polyunsaturated fatty acids (PUFAs)
OH
O
?
Lipid droplets
Stimulated Raman
Scattering signal
17β-HSD11/DHS-3::GFP
b
Stimulated Raman
Scattering (total lipids)
Head
Intestine
Control
fat-7 RNAi
ash-2 RNAi
fat-2 RNAi
High MUFAs
c
Lipid droplet number
<0.0001
<0.0001
60
40
20
0
Control
fat-7 RNAi
ash-2 RNAi
fat-2 RNAi
High MUFAs
d
Lipid droplet GFP
(DHS-3::GFP)
Head
Intestine
Control
fat-7 RNAi
ash-2 RNAi
fat-2 RNAi
High MUFAs
e
Lipid droplet number
0.0228
<0.0001
250
200
150
100
50
0
Control
fat-7 RNAi
ash-2 RNAi
fat-2 RNAi
High MUFAs
f
Males
Lipid droplet number
0.0080
100
80
60
40
20
0
Control
ash-2 RNAi
g
Hypodermal
lipid droplet-mCherry
(PLIN-1::mCherry)
PLIN-1::mCherry
Control
(example 1)
Control
(example 2)
ash-2 RNAi
fat-2 RNAi
h
Hypodermal lipid droplet number
ns
ns
150
100
50
0
Control
ash-2 RNAi
fat-2 RNAi
i
Oleic acid (olive oil, nuts)
OH
O
cis MUFA
Elaidic acid (margarine,
dairy)
trans MUFA
j
Lipid droplet GFP
(DHS-3::GFP)
Control
(example 1)
Control
(example 2)
Oleic acid
Elaidic acid
k
Lipid droplet number
<0.0001
<0.0001
300
200
100
0
Control
Oleic acid
Elaidic acid
l
Percent survival
Control
Oleic acid
Elaidic acid
+35%
<0.0001
ns
100
50
0
0
10
20
30
40
Age (days)
m
ATGL/
ATGL-1
HSL/
HOSL-1
3. Lipid droplet
degradation
LIPIN/
LPIN-1
SEIPIN/
SEIP-1
1. Triglyceride
synthesis
2. Lipid droplet
budding
n
Lipid droplet number
0.0006
ns
250
200
150
100
50
0
Control
ash-2 RNAi
lpin-1 RNAi
lpin-1/ash-2 RNAi
o
Lipid droplet number
0.0040
ns
400
300
200
100
0
Control
Oleic acid
lpin-1 RNAi
lpin-1 RNAi
+ Oleic acid
p
Percent survival
Control
ash-2 RNAi
lpin-1 RNAi
lpin-1/ash-2
RNAi
+33%
<0.0001
+17%
<0.0001
100
50
0
0
10
20
30
40
Age (days)
q
Percent survival
Control
Control
+ Oleic acid
lpin-1 RNAi
lpin-1 RNAi
+ Oleic acid
+18%
<0.0001
ns
100
50
0
0
10
20
30
40
Age (days)
r
Percent survival
WT control
WT ash-2 RNAi
seip-1(gk5008)
control
seip-1(gk5008)
ash-2 RNAi
+33%
<0.0001
ns
100
50
0
0
10
20
30
40
Age (days)
s
Percent survival
WT control
WT fat-2 RNAi
seip-1(gk5008)
control
seip-1(gk5008)
fat-2 RNAi
+32%
<0.0001
ns
100
50
0
0
10
20
30
40
50
Age (days)

Figure 1. Monounsaturated fatty acids lead to an increase in lipid droplet number and this is necessary for lifespan extension

a, Fatty acid synthesis pathway and lipid droplets in *C. elegans* and genetic or dietary interventions that lead to accumulation of endogenous monounsaturated fatty acids (MUFAs)[6,10]. The name of the mammalian proteins is also indicated.

b-c, Lipid droplet number and intensity, measured by Stimulated Raman Scattering (SRS) microscopy, in MUFA-enriched worms. **b,** Upper panel: SRS image of the anterior part of one worm (head and intestine). Scale bar = 100 µm. Lower panels: Zoomed-in SRS images of worms treated with control (empty vector) RNAi, *fat-7* RNAi (MUFA-depleted), and *ash-2* or *fat-2* RNAi (MUFA-enriched). Scale bar = 5 µm. **c,** Quantification of lipid droplet number, as assessed by SRS, of worms treated as in b. *n* ≥ 18 worms for each condition. Representative of two independent experiments (see Source Data Figure 1 for all experiments and statistics). Data are mean ± s.d. Each dot represents the lipid droplet number in a 26 x 26 μm^2 area in the intestine of an individual worm. *P*-values: two-tailed Mann-Whitney test. Lipid droplet intensity, as assessed by SRS, is quantified in Extended Data Fig. 1d.

d-e, Intestinal lipid droplet number, measured using the transgenic line strain expressing a fusion between the lipid droplet protein DHS-3 and GFP driven by the endogenous *dhs-3* promoter (intestinal expression) (*dhs-3p::dhs-3::GFP)*, in MUFA-enriched worms. **d,** Upper panel: Fluorescent image of the anterior part of one worm (Head and intestine). Scale bar = 100 µm. Lower panels: Zoomed-in fluorescent images of the mid-intestine area of worms treated with control (empty vector) RNAi, *fat-7* RNAi (MUFA-depleted), or *ash-2* or *fat-2* RNAi (MUFA-enriched). Scale bar = 5 µm. **e,** Quantification of lipid droplet number in worms treated as in d. *n* ≥ 12 worms for each condition. Representative of two independent experiments (see Source Data Figure 1 for all experiments and statistics). Data are mean ± s.d. Each dot represents the lipid droplet number in a 26 x 26 μm^2 area in the intestine of an individual worm. *P*-values: two-tailed Mann-Whitney test.

f, Quantification of lipid droplet number in males treated with control (empty vector) RNAi or *ash-2* RNAi (MUFA-enriched). *n* ≥ 22 worms for each condition. Representative of two independent experiments (see Source Data Figure 1 for all experiments and statistics). Data and *P*-values as in e.

g-h, Hypodermal lipid droplet number in MUFA-enriched worms, measured using the transgenic line strain expressing a fusion between PLIN-1 and mCherry driven by the endogenous *plin-1* promoter (hypodermal expression) (*plin-1::plin-1::mCherry*). **g,** Zoomed-in fluorescent image of the hypodermis of worms treated with control (empty vector) RNAi, or *ash-2* or *fat-2* RNAi (MUFA-enriched). Scale bar = 5 µm. **h,** Quantification of lipid droplet number in worms treated as in g. $n \geq 21$ worms for each condition. Representative of two independent experiments (see Source Data Figure 1 for all experiments and statistics). Data are mean ± s.d. Each dot represents the lipid droplet number in a 15 x 15 μm^2 area of an individual worm. *P*-values: two-tailed Mann-Whitney test.

i, Chemical structure of the cis MUFA oleic acid and the trans MUFA elaidic acid.

j-k, Cis MUFA (oleic acid), but not trans MUFA (elaidic acid), increases lipid droplet numbers. Intestinal lipid droplets measured by fluorescence in the *dhs-3p::dhs-3::GFP* transgenic line upon sterically different dietary MUFAs. **j**, Zoomed-in fluorescent images of the mid-intestine upon dietary oleic acid (cis fatty acid) or elaidic acid (trans fatty acid). Scale bar = 5 µm. **k**, Quantification of lipid droplet number in worms treated as in j. $n \geq 28$ worms for each condition. Representative of two independent experiments (see Source Data Figure 1 for all experiments and statistics). Data and *P*-values as in e.

l, Cis MUFA (oleic acid), but not trans MUFA (elaidic acid), extends lifespan. Kaplan Meier survival curve of worms treated as in j. $n \geq 128$ worms for each condition. Representative of two independent experiments (see Extended Data Table 1 for all lifespan experiments and statistics). Percentages of median lifespan extension and *P*-values are indicated on the right. *P*-values: log-rank Mantel-Cox test.

m, Conserved proteins involved in lipid droplet synthesis and degradation. The mammalian name is indicated first. LIPIN/LPIN-1 is part of the pathway that synthesizes the triglycerides packed in lipid droplets. SEIPIN/SEIP-1 assists the budding of mature lipid droplets from the endoplasmic reticulum. The lipases ATGL/ATGL-1 and HSL/HOSL-1 hydrolyze glycerolipids from lipid droplets.

n-o, *Lpin-1* is required for lipid droplet increase upon MUFA increase. Intestinal lipid droplet number, measured by fluorescence in the *dhs-3p::dhs-3::GFP* transgenic line, in MUFA-enriched and lipid droplet depleted worms. **n,** Quantification of lipid droplet number in worms treated with control (empty vector)*, ash-2*, *lpin-1,* or *ash-2/lpin-1* RNAi (see Extended Data Fig. 1k for efficiency of double knock-down). $n \geq 16$ worms for each condition. Representative of two independent experiments (see Source Data Figure 1 for all experiments and statistics). Data are mean ± s.d. Each dot represents the lipid droplet number in a 26 x 26 μm^2 area in the intestine of an individual worm. *P*-values*:* two-tailed Mann-Whitney test. **o,** *Lpin-1* is required for lipid droplet increase upon oleic acid supplementation. Quantification of lipid droplet number in worms treated with control (empty vector) or *lpin-1* RNAi upon dietary oleic acid. $n \geq 29$ worms for each condition. Representative of two independent experiments (see Source Data Figure 1 for all experiments and statistics). Data and *P*-values as in n.

p, *lpin-1* is necessary for longevity upon MUFA enrichment by *ash-2* depletion. Kaplan Meier survival curve of worms treated with control (empty vector), *ash-2, lpin-1, or ash-2/lpin-1* RNAi. $n \geq 96$ for each condition. Representative of two independent experiments (see Extended Data Table 1 for all lifespan experiments and statistics). Percentages of median lifespan extension and *P*-values are indicated on the right. *P*-values: log-rank Mantel-Cox test. *ash-2* and *lpin-1* RNAi significantly interact with each other using the Cox proportional hazard test (*P*-value= 0.0142).

q, *lpin-1* is required for longevity upon oleic acid supplementation. Kaplan Meier survival curve of worms treated with control (empty vector) or *lpin-1* RNAi upon dietary oleic acid. Representative of two independent experiments (see Extended Data Table 1 for all lifespan experiments and statistics). $n \geq 105$ worms for each condition. Percentages of median lifespan extension and *P*-values are indicated on the right. *P*-values: log-rank Mantel-Cox test. Oleic acid and *lpin-1* RNAi significantly interact with each other using the Cox proportional hazard test (*P*-value= 2.53e-07).

r*, seip-1* is required for MUFA-mediated longevity upon *ash-2* depletion. Kaplan Meier survival curve of wildtype and *seip-1(gk5008)* mutant worms treated with control (empty vector) or *ash-2* RNAi. $n \geq 64$ for each condition. Representative of three independent experiments (see Extended Data Table 1 for all lifespan experiments and statistics). Percentage of median lifespan extension and *P*-values are indicated on the right. *P*-values: log-rank Mantel-Cox test. *ash-2* RNAi and *seip-1* mutation significantly interact with each other using the Cox proportional hazard test (*P*-value=5.36e-10).

s, *seip-1* is required for MUFA-mediated longevity upon *fat-2* depletion. Kaplan Meier survival curve of wildtype and *seip-1(gk5008)* mutant worms treated with control (empty vector) or *fat-2* RNAi. $n \geq 90$ for each condition. Representative of two independent experiments (see Extended Data Table 1 for all lifespan experiments and statistics). Percentage of median lifespan extension and *P*-values are indicated on the right. *P*-values: log-rank Mantel-Cox test. *fat-2* RNAi and *seip-*

1 mutation significantly interact with each other using the Cox proportional hazard test (*P*-value= 9.07e-12).

All experiment data and statistics are shown in Source Data Figure 1. All lifespan data and statistics are shown in Extended Data Table 1.

Figure 2

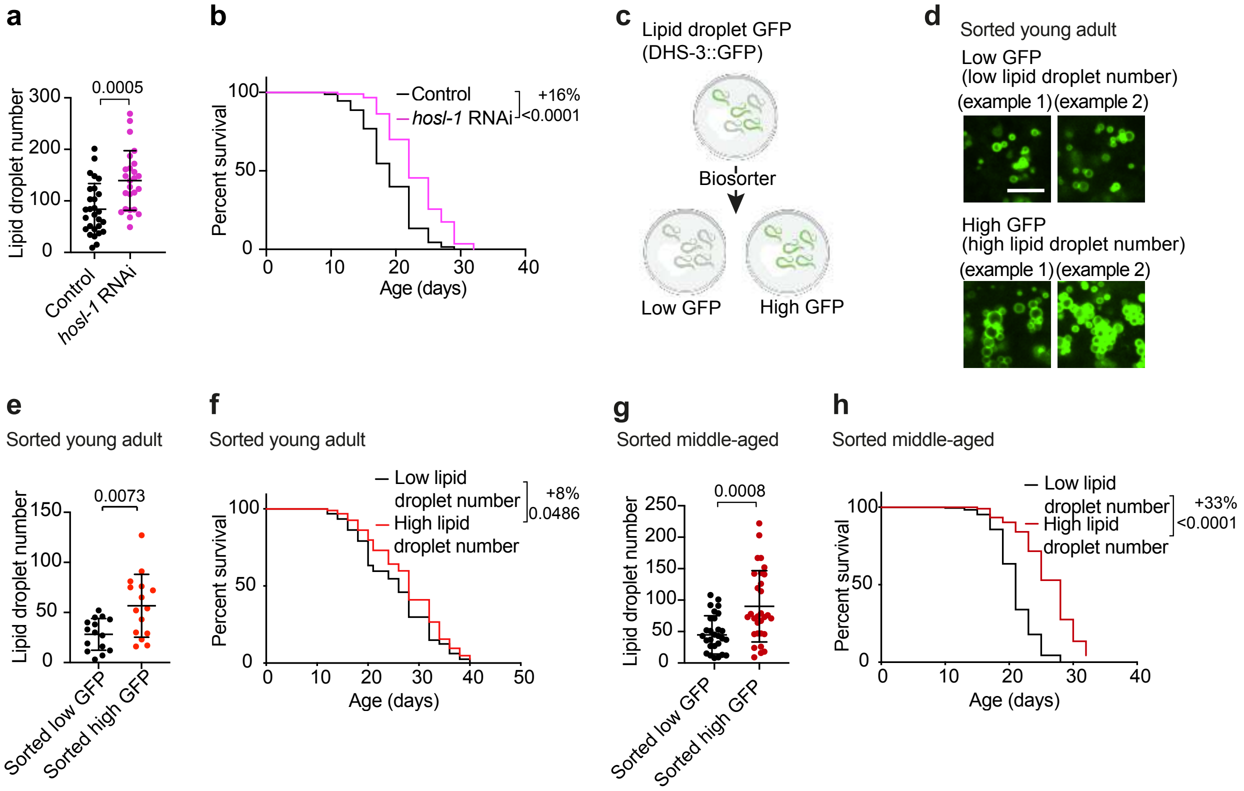

Figure 2. Increased lipid droplets are beneficial for longevity and predictive of a long life

a, *hosl-1* knockdown leads to increased lipid droplet number. Intestinal lipid droplet number, measured by fluorescence in the *dhs-3p::dhs-3::GFP* transgenic line, in worms with decreased lipid droplet degradation. Quantification of lipid droplet number in worms treated with control (empty vector) and *hosl-1* RNAi. *n* ≥ 28 worms for each condition. Representative of two independent experiments (see Source Data Figure 2 for all experiment data and statistics). Data are mean ± s.d. Each dot represents the lipid droplet number in a 26 x 26 μm^2 area in the intestine of an individual worm. *P*-values: two-tailed Mann-Whitney test.

b, *hosl-1* knockdown extends lifespan. Kaplan Meier survival curve of wildtype worms treated with control (empty vector) or *hosl-1* RNAi. n ≥ 94 for each condition. Representative of three independent experiments (see Extended Data Table 1 for all lifespan experiments and statistics). Percentages of median lifespan extension and *P*-values are indicated on the right. *P*-values: log-rank Mantel-Cox test.

c, Experiment setup for sorting worms according to the fluorescence intensity of the DHS-3::GFP lipid droplet reporter (as a proxy for lipid droplet number, see d-e) using the large particle BioSorter.

d-e, When sorted at young adult age, high fluorescent DHS-3::GFP worms have a higher intestinal lipid droplet number than low fluorescent worms. Lipid droplet number was assessed after BioSorting a synchronized population of young adult worms (adult day 1) of the *dhs-3p::dhs-3::GFP* transgenic line. **d,** Zoomed-in fluorescent images of the mid-intestine area. Scale bar = 5 µm. **e,** Quantification of lipid droplet number in worms sorted as in d. $n \geq 15$ worms for each condition. Representative of two independent experiments (see Source Data Figure 2 for all experiment data and statistics). Data and *P*-values as in a.

f, Worms sorted at young adult age with high lipid droplet number live longer than worms with a low lipid droplet number. Kaplan Meier survival curve of age-synchronized wildtype worms BioSorted according to their lipid droplet intensity (a proxy for increased lipid droplet number, see e). Representative of two independent experiments (see Extended Data Table 1 for all lifespan experiments and statistics). $n \geq 117$ worms for each condition. The percentage of median lifespan extension are indicated on the right. *P*-values: log-rank Mantel-Cox test.

g, When sorted at middle age, high fluorescent DHS-3::GFP worms have a higher intestinal lipid droplet number than low fluorescent worms. Lipid droplet number was assessed after manual sorting of a synchronized population of middle-aged adult worms (adult day 6) of the *dhs-3p::dhs-3::GFP* transgenic line. Because the BioSorter requires a high number of worms as an input and because the retrieval of sufficiently high enough worm numbers at old age can be very labor intensive, manual sorting was performed instead. $n \geq 30$ worms for each condition. Representative of two independent experiments (see Source Data Figure 2 for all experiment data and statistics). Data and *P*-values as in a. Zoomed-in images shown in Extended Data Fig 2d.

h, Worms sorted at middle age with high lipid droplet number live longer than worms with a low lipid droplet number. Kaplan Meier survival curve of age-synchronized wildtype worms manually sorted according to their lipid droplet intensity (a proxy for increased lipid droplet number, see g). $n \geq 195$ worms for each condition. Representative of three independent experiments (see Extended Data Table 1 for all lifespan experiments and statistics). Percentages of median lifespan extension and *P*-values are indicated on the right. *P*-values: log-rank Mantel-Cox test.

All experiment data and statistics are in Source Data Figure 2. All lifespan data and statistics are in Extended Data Table 1.

Figure 3

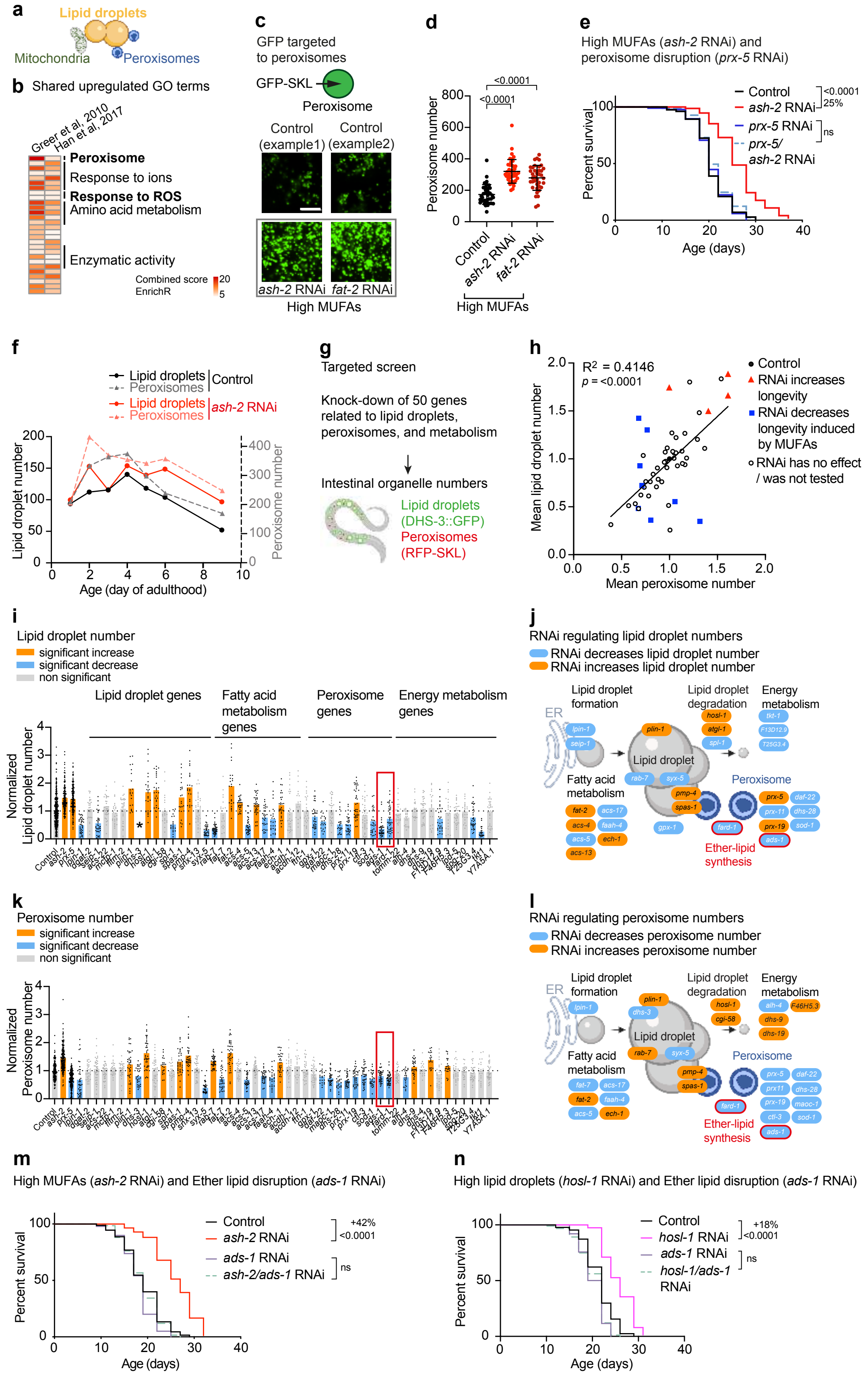
a
Lipid droplets
Mitochondria
Peroxisomes
b Shared upregulated GO terms
Greer et al, 2010
Han et al, 2017
Peroxisome
Response to ions
Response to ROS
Amino acid metabolism
Enzymatic activity
Combined score EnrichR
20
5
c
GFP targeted to peroxisomes
GFP-SKL
Peroxisome
Control (example1)
Control (example2)
ash-2 RNAi
fat-2 RNAi
High MUFAs
d
Peroxisome number
<0.0001
<0.0001
Control
ash-2 RNAi
fat-2 RNAi
High MUFAs
e
High MUFAs (ash-2 RNAi) and peroxisome disruption (prx-5 RNAi)
Percent survival
Age (days)
Control
ash-2 RNAi
prx-5 RNAi
prx-5/ ash-2 RNAi
<0.0001
25%
ns
f
Lipid droplets
Peroxisomes
Control
Lipid droplets
Peroxisomes
ash-2 RNAi
Lipid droplet number
Peroxisome number
Age (day of adulthood)
g
Targeted screen
Knock-down of 50 genes related to lipid droplets, peroxisomes, and metabolism
Intestinal organelle numbers
Lipid droplets (DHS-3::GFP)
Peroxisomes (RFP-SKL)
h
R² = 0.4146
p = <0.0001
Control
RNAi increases longevity
RNAi decreases longevity induced by MUFAs
RNAi has no effect / was not tested
Mean lipid droplet number
Mean peroxisome number
i
Lipid droplet number
significant increase
significant decrease
non significant
Lipid droplet genes
Fatty acid metabolism genes
Peroxisome genes
Energy metabolism genes
Normalized Lipid droplet number
j
RNAi regulating lipid droplet numbers
RNAi decreases lipid droplet number
RNAi increases lipid droplet number
ER
Lipid droplet formation
Lipid droplet degradation
Energy metabolism
Lipid droplet
Fatty acid metabolism
Peroxisome
Ether-lipid synthesis
k
Peroxisome number
significant increase
significant decrease
non significant
Normalized Peroxisome number
l
RNAi regulating peroxisome numbers
RNAi decreases peroxisome number
RNAi increases peroxisome number
m
High MUFAs (ash-2 RNAi) and Ether lipid disruption (ads-1 RNAi)
Control
ash-2 RNAi
ads-1 RNAi
ash-2/ads-1 RNAi
+42%
<0.0001
ns
Percent survival
Age (days)
n
High lipid droplets (hosl-1 RNAi) and Ether lipid disruption (ads-1 RNAi)
Control
hosl-1 RNAi
ads-1 RNAi
hosl-1/ads-1 RNAi
+18%
<0.0001
ns
Percent survival
Age (days)

Figure 3. Functional peroxisomes and ether lipid synthesis are required for lipid droplets to extend lifespan in response to MUFAs

a, Organelles such as mitochondria and peroxisomes are in close contact with lipid droplets to regulate lipid metabolism.

b, Re-analysis of transcriptomic datasets of worms with or without MUFA accumulation[5,6]. Shared upregulated GO terms between worms treated with control (empty vector) and *ash-2* RNAi. GO terms were analyzed using WormEnrichR[29,123]. Left column: GO terms upregulated in middle aged individuals (post-reproductive, adult day 6/ whole worms)[5]. Right column: GO terms upregulated in young individuals (adult day 1/ intestine)[6]. GO terms were considered significant if they have a combined score of log *P*-value (Fisher's exact test) multiplied with rank-based enrichment z-score larger than 5 (Ref [122-124]). See Extended Data Table 2 for all GO terms and classifications.

c-d, Peroxisome number increases in MUFA-enriched worms. Intestinal peroxisomes measured by fluorescence in the *ges-1p::GFP-SKL* transgenic line, which expresses a peroxisome-localized GFP driven by the intestinal *ges-1* promoter. **c,** Zoomed-in fluorescent images of the last intestinal cell in worms treated with control (empty vector) RNAi or *ash-2* or *fat-2* RNAi (MUFA-enriched). Scale bar = 5 µm. Intensity of peroxisome-localized GFP quantified in Extended Data Fig 3a.

d, Quantification of peroxisome number in worms treated with control (empty vector) RNAi or *ash-2* or *fat-2* RNAi (MUFA-enriched). $n \geq 35$ worms for each condition. Representative of three independent experiments (see Source Data Figure 3 for all experiment data and statistics). Data are mean ± s.d. Each dot represents the peroxisome number in a 26 x 26 μm^2 area in the intestine of an individual worm. *P*-values*:* two-tailed Mann-Whitney test.

e, *prx-5* is necessary for longevity upon MUFA enrichment by *ash-2* depletion. Kaplan Meier survival curve of worms treated with control (empty vector), *ash-2, prx-5*, or *ash-2/prx-5* RNAi. $n \geq 94$ for each condition. Representative of two independent experiments (see Extended Data Table 1 for all lifespan experiments and statistics). Percentages of median lifespan extension and *P*-values are indicated on the right. *P*-values: log-rank Mantel-Cox test. *ash-2* and *prx-5* RNAi significantly interact with each other using the Cox proportional hazard test (*P*-value= 4.02e-06).

f, Lipid droplet and peroxisome accumulation/degradation follow similar dynamics with age. Intestinal peroxisomes and lipid droplets measured by fluorescence in the *dhs-3p::dhs-3::GFP*, *vha-6p::mRFP-SKL* transgenic line in MUFA-enriched worms. This transgenic line expresses both the lipid droplet marker DHS-3 fused to GFP driven by the *dhs-3* promoter (intestine) and a peroxisome localized-mRFP driven by the *vha-6* promoter (intestine). Quantification of organelle numbers in worms treated with control (empty vector) or *ash-2* RNAi. $n \geq 23$ worms for each condition. Representative of two independent experiments (see Source Data Figure 3 for all experiment data and statistics). Each dot represents the mean organelle number in a 26 x 26 μm^2 area in the intestine of all worms imaged for this condition. Left y-axis: lipid droplet number, right y-axis: peroxisome number.

g, Design of targeted screen to test for effect of specific genes on lipid droplet and peroxisome number.

h, Lipid droplet and peroxisome numbers correlate in the screen. Intestinal peroxisomes and lipid droplets measured by fluorescence in the *dhs-3p::dhs-3::GFP*, *vha-6p::mRFP-SKL* transgenic line. Quantification of organelle numbers in worms treated with 50 different RNAis (see Source Data Figure 3 for all experiment data and statistics). $n \geq 15$ worms for each condition. Each dot represents the mean organelle number in a 26 x 26 μm^2 area in the intestine of all worms imaged for this condition normalized to the control mean. Black: Control (empty vector) RNAi. Red: RNAi conditions that increase longevity. Blue: RNAi conditions that decrease longevity upon MUFAs. White: RNAi conditions that have no effects on longevity or were not tested. Correlation: Pearson R^2 test.

i, j Genes that influence lipid droplet number. **i,** Intestinal lipid droplets measured by fluorescence in the *dhs-3p::dhs-3::GFP*, *vha-6p::mRFP-SKL* transgenic line. Quantification of lipid droplet number in worms treated with 50 different RNAis (see Source Data Figure 3 for all experiment data and statistics). $n \geq 15$ worms for each condition. Data are mean ± s.d. Each dot represents the organelle number in a 26 x 26 μm^2 area in the intestine of an individual worm normalized to control worms. Orange: significant increase in lipid droplet number, light blue: significant decrease in lipid droplet number. Conditions are colored if the adjusted *P*-value < 0.05 using the unpaired Wilcoxon test with Benjamini-Hochberg test for multiple hypothesis correction. (*) *dhs-3* RNAi abolishes the GFP signal of the lipid droplet DHS-3::GFP reporter. **j,** Genes that regulate of lipid droplet numbers found in i. Orange: significant increase in lipid droplet number, light blue: significant decrease in lipid droplet number.

k, l Genes that influence peroxisome number. **k,** Intestinal peroxisome measured by fluorescence in the *dhs-3p::dhs-3::GFP*, *vha-6p::mRFP-SKL* transgenic line. Quantification of peroxisome number in worms treated with 50 different RNAis (see Source Data Figure 3 for all experiment data and statistics). $n \geq 19$ worms for each condition. Data are mean ± s.d. Each dot represents the organelle number in a 26 x 26 μm^2 area in the intestine of an individual worm normalized to control worms. Orange: significant increase peroxisome number, light blue: significant decrease in peroxisome number. Conditions are colored if the adjusted *P*-value < 0.05 using the unpaired Wilcoxon test with Benjamini-Hochberg test for multiple hypothesis correction. **l,** Genes that regulate of peroxisome numbers found in k. Orange: significant increase in peroxisome number, light blue: significant decrease in peroxisome number.

m, *ads-1*, a gene involved in ether lipid synthesis, is necessary for longevity upon MUFA enrichment by *ash-2* depletion. Kaplan Meier survival curve of worms treated with control (empty vector), *ash-2, ads-1*, or *ash-2/ads-1* RNAi. $n \geq 81$ for each condition. Representative of two independent experiments (see Extended Data Table 1 for all lifespan experiments and statistics). Percentages of median lifespan extension and *P*-values are indicated on the right. *P*-values: log-rank Mantel-Cox test. *ash-2* and *ads-1* RNAi significantly interact with each other using the Cox proportional hazard test (*P*-value= 1.28e-07).

n, *ads-1*, a gene involved in ether lipid synthesis, is necessary for longevity upon lipid droplet enrichment by *hosl-1* depletion. Kaplan Meier survival curve of worms treated with control (empty vector), *hosl-1, ads-1*, or *hosl-1/ads-1* RNAi. $n \geq 94$ for each condition. Representative of two independent experiments (see Extended Data Table 1 for all lifespan experiments and statistics). Percentages of median lifespan extension and *P*-values are indicated on the right. *P*-values: log-rank Mantel-Cox test. *hosl-1* and *ads-1* RNAi significantly interact with each other using the Cox proportional hazard test (*P*-value= 1.23e-06). Control lifespan curves are also shown in Fig. 2h.

All experiment data and statistics are in Source Data Figure 3. All lifespan data are in Extended Data Table 1.

Figure 4

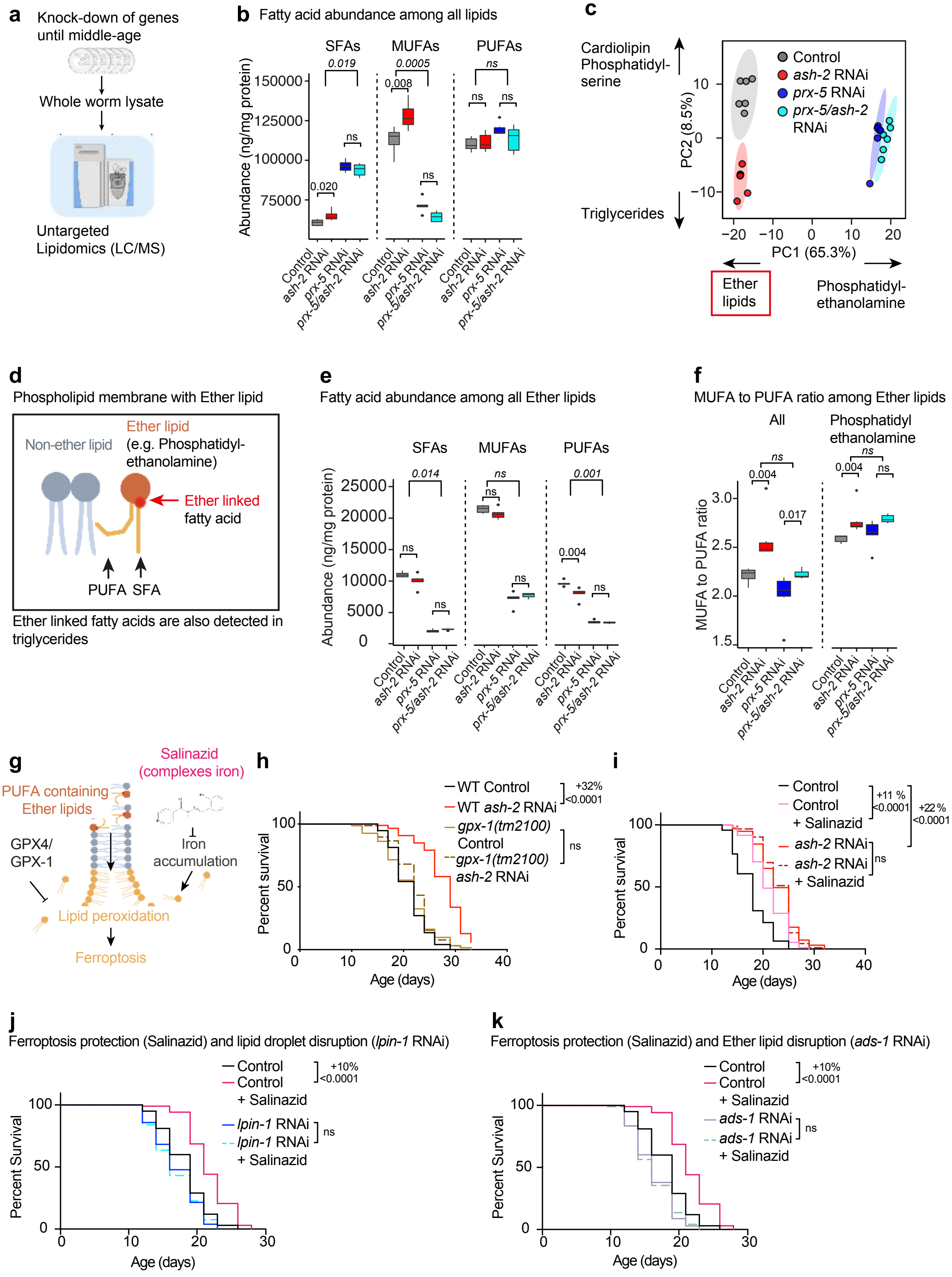
a
Knock-down of genes until middle-age
Whole worm lysate
Untargeted Lipidomics (LC/MS)
b
Fatty acid abundance among all lipids
SFAs
MUFAs
PUFAs
Abundance (ng/mg protein)
150000
125000
100000
75000
0.019
0.020
ns
0.0005
0.008
ns
ns
ns
ns
Control
ash-2 RNAi
prx-5 RNAi
prx-5/ash-2 RNAi
c
Cardiolipin
Phosphatidyl-serine
Triglycerides
PC2 (8.5%)
10
0
−10
−20
−10
0
10
20
PC1 (65.3%)
Ether lipids
Phosphatidyl-ethanolamine
Control
ash-2 RNAi
prx-5 RNAi
prx-5/ash-2 RNAi
d
Phospholipid membrane with Ether lipid
Non-ether lipid
Ether lipid (e.g. Phosphatidyl-ethanolamine)
Ether linked fatty acid
PUFA
SFA
Ether linked fatty acids are also detected in triglycerides
e
Fatty acid abundance among all Ether lipids
SFAs
MUFAs
PUFAs
Abundance (ng/mg protein)
25000
20000
15000
10000
5000
0
0.014
ns
ns
ns
ns
ns
0.001
0.004
ns
Control
ash-2 RNAi
prx-5 RNAi
prx-5/ash-2 RNAi
f
MUFA to PUFA ratio among Ether lipids
All
Phosphatidyl ethanolamine
MUFA to PUFA ratio
3.0
2.5
2.0
1.5
ns
0.004
0.017
ns
0.004
ns
Control
ash-2 RNAi
prx-5 RNAi
prx-5/ash-2 RNAi
g
Salinazid (complexes iron)
PUFA containing Ether lipids
GPX4/ GPX-1
Iron accumulation
Lipid peroxidation
Ferroptosis
h
WT Control
WT ash-2 RNAi
gpx-1(tm2100) Control
gpx-1(tm2100) ash-2 RNAi
+32%
<0.0001
ns
Percent survival
100
50
0
0
10
20
30
40
Age (days)
i
Control
Control + Salinazid
ash-2 RNAi
ash-2 RNAi + Salinazid
+11 %
<0.0001
+22%
<0.0001
ns
Percent survival
100
50
0
0
10
20
30
40
Age (days)
j
Ferroptosis protection (Salinazid) and lipid droplet disruption (lpin-1 RNAi)
Control
Control + Salinazid
lpin-1 RNAi
lpin-1 RNAi + Salinazid
+10%
<0.0001
ns
Percent Survival
100
50
0
0
10
20
30
Age (days)
k
Ferroptosis protection (Salinazid) and Ether lipid disruption (ads-1 RNAi)
Control
Control + Salinazid
ads-1 RNAi
ads-1 RNAi + Salinazid
+10%
<0.0001
ns
Percent Survival
100
50
0
0
10
20
30
Age (days)

Figure 4. Ether lipid changes upon MUFA supplementation and role of ferroptosis in MUFA-mediated longevity

a, Untargeted lipidomic analysis on whole worms using liquid chromatography/mass spectrometry (LC/MS). Middle-aged worms (adult day 6) treated with control (empty vector), *ash-2*, *prx-5*, or *ash-2/prx-5* RNAi were lyzed, and whole-worm lysates were subjected to LC/MS. Six biological replicates with ~500 individual worms per condition.

b, Fatty acid abundance of saturated fatty acids (SFAs), monounsaturated fatty acids (MUFAs) and polyunsaturated fatty acids (PUFAs) among all lipids in middle-aged worms treated with control (empty vector), *ash-2*, *prx-5*, or *ash-2/prx-5* RNAi. Box and whisker plot, with median (central line), 25th and 75th percentile (outer lines), and minimum and maximum within 1.5 times the interquartile range (whiskers). Values beyond these are considered outliers and plotted individually. Complete list of fatty acid categories and statistics is in (Source Data Figure 4). *P*-values: Unpaired two-samples Wilcoxon test with Benjamini-Hochberg test for multiple hypothesis correction. Italic *P*-values: two-way ANOVA.

c, Principal component analysis (PCA) on the lipidome separates MUFA-enriched conditions (*ash-2* RNAi) from control conditions and from conditions in which peroxisomes are depleted (*prx-5* and *prx-5/ash-2* RNAi). Each dot represents a biological replicate. Six biological replicates of ~500 individual worms per condition. Complete list of all lipids driving the PCA separation available is in (Extended Data Table 3).

d, Ether lipids are mostly located in membranes. Ether lipids contain one fatty acid that is attached via an ether-bond to the head group (red circle). Ether lipids are present in several lipid classes, but are enriched in membrane lipids (e.g. phosphatidylethanolamine, PE). Complete list of detected ether lipids and statistics is in (Source Data Extended Data Figure 4).

e, Fatty acid abundance of saturated fatty acids (SFAs), monounsaturated fatty acids (MUFAs) and polyunsaturated fatty acids (PUFAs) among ether lipids in middle-aged worms treated as in a. Box and whisker plot, with median (central line), 25th and 75th percentile (outer lines), and minimum and maximum within 1.5 times the interquartile range (whiskers). Values beyond these are considered outliers and plotted individually. Complete list of fatty acid categories and statistics is in (Source Data Figure 4). *P*-values: Unpaired two-samples Wilcoxon test with Benjamini-Hochberg test for multiple hypothesis correction. Italic *P*-values: two-way ANOVA.

f, MUFA to PUFA ratio among all ether lipids (left panel) and among ether lipids in phosphatidylethanolamine (PE, right panel) in worms treated as in a. Data and statistics as in b.

The PE panel is also in Extended Data Fig. 4e. Complete list of the MUFA to PUFA ratios and statistics can be found in (Source Data Figure 4).

g, Strategies to inhibit ferroptosis. GPX4/GPX-1 protects cells against membrane peroxidation by degrading lipid peroxides. The chemical Salinazid complexes iron, thereby blocking toxic iron accumulation and ferroptosis.

h, *gpx-1* is necessary for longevity upon MUFA enrichment by *ash-2* depletion. Kaplan Meier survival curve of *gpx-1(tm21000)* or wildtype worms treated with control (empty vector) or *ash-2* RNAi. n ≥ 82 for each condition. Representative of two independent experiments (see Extended Data Table 1 for all lifespan experiments and statistics). Percentages of median lifespan extension and *P*-values are indicated on the right. *P*-values: log-rank Mantel-Cox test. *Gpx-1(tm21000)* and *ash-2* RNAi significantly interact with each other using the Cox proportional hazard test (*P*-value= 3.4e-09).

i, Ferroptosis protection does not further increase MUFA-mediated longevity. Kaplan Meier survival curve of worms treated with control (empty vector) or *ash-2* RNAi upon Salinazid. n ≥ 110 for each condition. Percentages of median lifespan extension and *P*-values are indicated on the right. *P*-values: log-rank Mantel-Cox test. *ash-2* RNAi and Salinazid significantly interact with each other using the Cox proportional hazard test (*P*-value= 2.10e-06). Representative of one independent experiment (see Extended Data Table 1 for all lifespan experiments and statistics). Controls are also plotted in Extended Data Fig. 4f.

j, Lipid droplets are necessary for longevity upon ferroptosis inhibition by Salinazid. Kaplan Meier survival curve of worms treated with control (empty vector) or *lpin-1* RNAi upon Salinazid. n ≥ 105 for each condition. Percentages of median lifespan extension and *P*-values are indicated on the right. *P*-values: log-rank Mantel-Cox test. *Lpin-1* RNAi and Salinazid significantly interact with each other using the Cox proportional hazard test (*P*-value= 1.79e-05). Representative of two independent experiments (see Extended Data Table 1 for all lifespan experiments and statistics). Controls are also plotted in k.

k, Ether lipids are necessary for longevity upon ferroptosis inhibition by Salinazid. Kaplan Meier survival curve of worms treated with control (empty vector) or *ads-1* RNAi upon Salinazid. n ≥ 105 for each condition. Percentages of median lifespan extension and *P*-values are indicated on the right. *P*-values: log-rank Mantel-Cox test. *ads-1* RNAi and Salinazid significantly interact with each other using the Cox proportional hazard test (*P*-value= 4.41e-05). Representative of two independent experiments (see Extended Data Table 1 for all lifespan experiments and statistics). Controls are also plotted in j.

All experiment data and statistics are in Source Data Figure 4. All lifespan data and statistics are in Extended Data Table 1.

Supplementary Files

This is a list of supplementary files associated with this preprint. Click to download.

- KP20210622ExtendedDataTable1Lifespandata.xlsx
- KP20210618ExtendedDataTable2GOterms.xlsx
- KP20210618ExtendedDataTable3PCAloadings.xlsx
- KP20210621ExtendedDataTable4Wormstrains.xlsx
- KP20210621ExtendedDataTable5qPCRprimer.xlsx
- KP20210621ExtendedDataTable6LipidomicData.xlsx
- KP20210720ExtendedDataTable7Fattyacidlength.xlsx
- PapsdorfetalExtendedData.pdf